

University of Groningen

Discovery of highly potent HDAC8 PROTACs with anti-tumor activity

Zhao, Chunlong; Chen, Deng; Suo, Feng-zhi; Setroikromo, Rita; Quax, Wim J.; Dekker, Frank

Published in:
 Bioorganic Chemistry

DOI:
[10.1016/j.bioorg.2023.106546](https://doi.org/10.1016/j.bioorg.2023.106546)

IMPORTANT NOTE: You are advised to consult the publisher's version (publisher's PDF) if you wish to cite from it. Please check the document version below.

Document Version
 Publisher's PDF, also known as Version of record

Publication date:
 2023

[Link to publication in University of Groningen/UMCG research database](#)

Citation for published version (APA):

Zhao, C., Chen, D., Suo, F., Setroikromo, R., Quax, W. J., & Dekker, F. (2023). Discovery of highly potent HDAC8 PROTACs with anti-tumor activity. *Bioorganic Chemistry*, 136, Article 106546. <https://doi.org/10.1016/j.bioorg.2023.106546>

Copyright

Other than for strictly personal use, it is not permitted to download or to forward/distribute the text or part of it without the consent of the author(s) and/or copyright holder(s), unless the work is under an open content license (like Creative Commons).

The publication may also be distributed here under the terms of Article 25fa of the Dutch Copyright Act, indicated by the "Taverne" license. More information can be found on the University of Groningen website: <https://www.rug.nl/library/open-access/self-archiving-pure/taverne-amendment>.

Take-down policy

If you believe that this document breaches copyright please contact us providing details, and we will remove access to the work immediately and investigate your claim.

Downloaded from the University of Groningen/UMCG research database (Pure): <http://www.rug.nl/research/portal>. For technical reasons the number of authors shown on this cover page is limited to 10 maximum.



Discovery of highly potent HDAC8 PROTACs with anti-tumor activity

Chunlong Zhao, Deng Chen, Fengzhi Suo, Rita Setroikromo, Wim J. Quax, Frank J. Dekker*

Department of Chemical and Pharmaceutical Biology, Groningen Research Institute of Pharmacy (GRIP), University of Groningen, Antonius Deusinglaan 1, 9713AV Groningen, The Netherlands

ARTICLE INFO

Keywords:

Histone deacetylase 8 (HDAC8)
Proteolysis Targeting Chimeras (PROTACs)
Triple-Negative Breast Cancer (TNBC)
Migration
T-cell leukemia
Apoptosis

ABSTRACT

Various diseases are deeply associated with aberrations in HDAC8 functions. These aberrations can be assigned to either structural functions or catalytic functions of HDAC8. Therefore, development of HDAC8 degradation inducers might be more promising than HDAC8 inhibitors. We employed the proteolysis targeting chimera (PROTAC) strategy to develop a selective and potent HDAC8 degradation inducer **CT-4** with single-digit nanomolar DC₅₀ values and over 95% D_{max} in both triple-negative breast cancer MDA-MB-231 cells and T-cell leukemia cells. Notably, **CT-4** demonstrated potent anti-migration activity and limited anti-proliferative activity in MDA-MB-231 cells. In contrast, **CT-4** effectively induced apoptotic cell death in Jurkat cells, as assessed by a caspase 3/7 activity assay and flow cytometry. Our findings suggest that the development of HDAC8 degradation inducers holds great potential for the treatment of HDAC8-related diseases.

1. Introduction

Histone deacetylases (HDACs) catalyze deacetylation of proteins lysine residues, which plays essential roles in regulation of gene expression and protein activity [1–3]. Eleven zinc-dependent HDACs and seven nicotinamide adenine dinucleotide (NAD⁺)-dependent sirtuins (SIRT) have been identified in humans. The zinc-dependent HDACs can be subdivided into four enzyme groups: class I (HDAC1, 2, 3, and 8), class IIa (HDAC4, 5, 7, and 9), class IIb (HDAC6 and 10), and class IV (HDAC11). The dysregulation of HDACs is deeply related to various cancers, inflammation, and neurodegenerative disorders [1,2]. Although four non-selective and one class-selective HDAC inhibitors have been approved for the treatment of cancers, especially for hematological malignancies [1,2], these HDAC inhibitors can cause serious side effects, probably owing to their broad-spectrum activity against HDACs [4,5]. Therefore, targeting specific HDAC isoforms may enable avoiding undesirable side effects, which will enable widening of the therapeutic indexes in contrast to non-selective and class-selective HDAC inhibitors.

HDAC8 is a unique class I HDAC containing 377 amino acids and can be located in both the nucleus and the cytoplasm [6–8]. Currently, it remains controversial whether histones are *bona fide* HDAC8 substrates [6,7]. Importantly, various non-histone proteins, such as Structural Maintenance of Chromosomes protein 3 (SMC3), Estrogen-Related Receptor alpha (ERR α), and p53 were reported to be either substrates or interaction partners of HDAC8 [6,7,9]. Apart from being a deacetylase, HDAC8 may also mediate signaling via scaffolding functions. For example, HDAC8 might act both as a deacetylase and an interacting scaffold in inv (16) fusion protein/HDAC8/p53 complex [10]. Additionally, HDAC8 can also interact with transcription factors including Signal Transducer and Activator of Transcription 3 (STAT3), cAMP Response Element-Binding protein (CREB) and Deleted in Esophageal Cancer 1 (DEC1) to regulate gene expression [11–13]. Aberrant HDAC8 expression or dysregulated interactions with transcription factors are deeply associated with various cancers, including T-cell malignancies, childhood neuroblastoma, breast cancer, colon cancer, and lung cancer [6–8,14–16]. In addition, HDAC8 is indispensable for the expression of p53, and depletion or inhibition of HDAC8 only affects the proliferation

Abbreviations: CRBN, cereblon; CREB, cAMP response element-binding protein; DCM, dichloromethane; DEC1, deleted in esophageal cancer 1; DIPEA, *N,N*-diisopropylethylamine; DMF, *N,N*-dimethylformamide; EDCl, 1-Ethyl-3-(3-dimethylaminopropyl)carbodiimide; ERR α , estrogen-related receptor alpha; HDAC, histone deacetylase; HATU, 1-[Bis(dimethylamino)methylene]-1H-1,2,3-triazolo[4,5-*b*]pyridinium 3-oxide hexafluorophosphate; HOBT, hydroxybenzotriazole; MTS, 3-(4,5-dimethylthiazol-2-yl)-5-(3-carboxymethoxyphenyl)-2-(4-sulfophenyl)-2H-tetrazolium; MeOH, methanol; NAD⁺, nicotinamide adenine dinucleotide; POI, protein of interest; PROTAC, proteolysis targeting chimera; SMC3, structural maintenance of chromosomes protein 3; STAT3, signal transducer and activator of transcription 3; TFA, trifluoroacetic acid; THF, tetrahydrofuran; TNBC, triple-negative breast cancer.

* Corresponding author.

E-mail address: f.j.dekker@rug.nl (F.J. Dekker).

<https://doi.org/10.1016/j.bioorg.2023.106546>

Received 27 January 2023; Received in revised form 11 April 2023; Accepted 12 April 2023

Available online 17 April 2023

0045-2068/© 2023 The Author(s). Published by Elsevier Inc. This is an open access article under the CC BY license (<http://creativecommons.org/licenses/by/4.0/>).

of cancer cells harboring mutated p53 [17]. Therefore, HDAC8 has emerged as a potentially attractive drug target for the treatment of various cancers. Over the past years, some HDAC8-selective inhibitors have been reported (Fig. 1A) [18–23].

Triple-Negative Breast Cancer (TNBC) is the most aggressive subtype of breast cancer, which accounts for 15% of all breast cancer cases and 25% of all breast cancer-related deaths [24]. However, no effective targeted therapy has been well-established so far [24]. HDAC8 is up-regulated in TNBC and is correlated with poor prognosis. However, its exact functions in TNBC were not fully elucidated [25]. Interestingly, pharmacological inhibition of HDAC8 showed limited anti-proliferative activity against solid tumor cells, including TNBC, whereas it clearly induced growth inhibition in T-cell malignancies [19,25]. Research have demonstrated that both deacetylase activity and the scaffolding function of HDAC8 play an essential role in metastasis of breast cancer cells. On the one hand, HDAC8 can trigger the dissemination of breast cancer cells via AKT/GSK-3 β /Snail signals [25]. On the other hand, HDAC8 can provide a scaffold platform for the HDAC8/SMAD3/4 heterotrimer complex to promote cell survival and migration in breast cancer cells [26]. However, it remains unclear whether the scaffolding function of HDAC8 contributes to proliferation of TNBC. In addition, although HDAC8-selective inhibitors demonstrates potent HDAC8 inhibition with two-digit nanomolar IC₅₀ values, their anti-proliferative activities against T-cell malignancies or neuroblastoma cells remained poor with two-digit micromolar GI₅₀ values [18,21,23]. These indicate that targeting of the HDAC8 deacetylase enzyme activity might not be sufficient, and instead, targeting of the scaffolding role of HDAC8 is needed to identify its roles in the pathology in TNBC and other HDAC8-related diseases.

Development of Proteolysis Targeting Chimeras (PROTACs) has

emerged as a novel and powerful strategy in drug discovery. PROTACs are heterobifunctional molecules consisting of a ligand for the protein of interest (POI), a ligand for E3 ligase, and a linker [27–29]. This heterobifunctional character enables simultaneous binding to the POI and E3 ligase to form a ternary complex, thus triggering target protein degradation via the Ubiquitin-Proteasome System (UPS) (Fig. 1B) [27,28]. The event-driven PROTACs enable inhibition of protein scaffolding functions or protein–protein interactions, thus enabling exploitation of protein functions that were considered to be undruggable by classical occupancy-driven therapeutics [30–32]. In recent years, some HDAC PROTACs have been reported, demonstrating the great therapeutic potential for the treatment of HDACs related diseases [33–43]. In 2022, several HDAC8 PROTACs were reported (Fig. 1C). Suzuki's group reported the first HDAC8 PROTAC 5 by connecting HDAC8 selective inhibitor to E3 ligase cereblon (CRBN) recruiter via different linkers [44]. Although PROTAC 5 potentially inhibited the growth of T-cell leukemia Jurkat cells, the degrading potency of PROTAC 5 against HDAC8 remained limited with a potency (DC₅₀ value) in the high nanomolar range (702 nM) in Jurkat cells [44]. Similarly, Sippl's group reported another HDAC8 PROTAC 6 with anti-neuroblastoma activity, which has poor efficiency to lower the HDAC8 levels in neuroblastoma cells [45]. Chen's group reported a class of HDAC8 PROTACs, including PROTAC 7 with a potency in the nanomolar range but provides recovery of the HDAC8 levels in 24 h in colorectal cancer cells [46]. Very recently, Zhu's group reported a new HDAC8 PROTAC 8, which provided a DC₅₀ value of 580 nM in A549 cells, but demonstrated limited HDAC8-degrading ability in Jurkat cells [47]. In addition, PROTAC 8 showed slightly better *in vitro* anti-proliferative activity against A549 cells than HDAC8 inhibitor 1 [47]. This indicates the need to explore structure–function

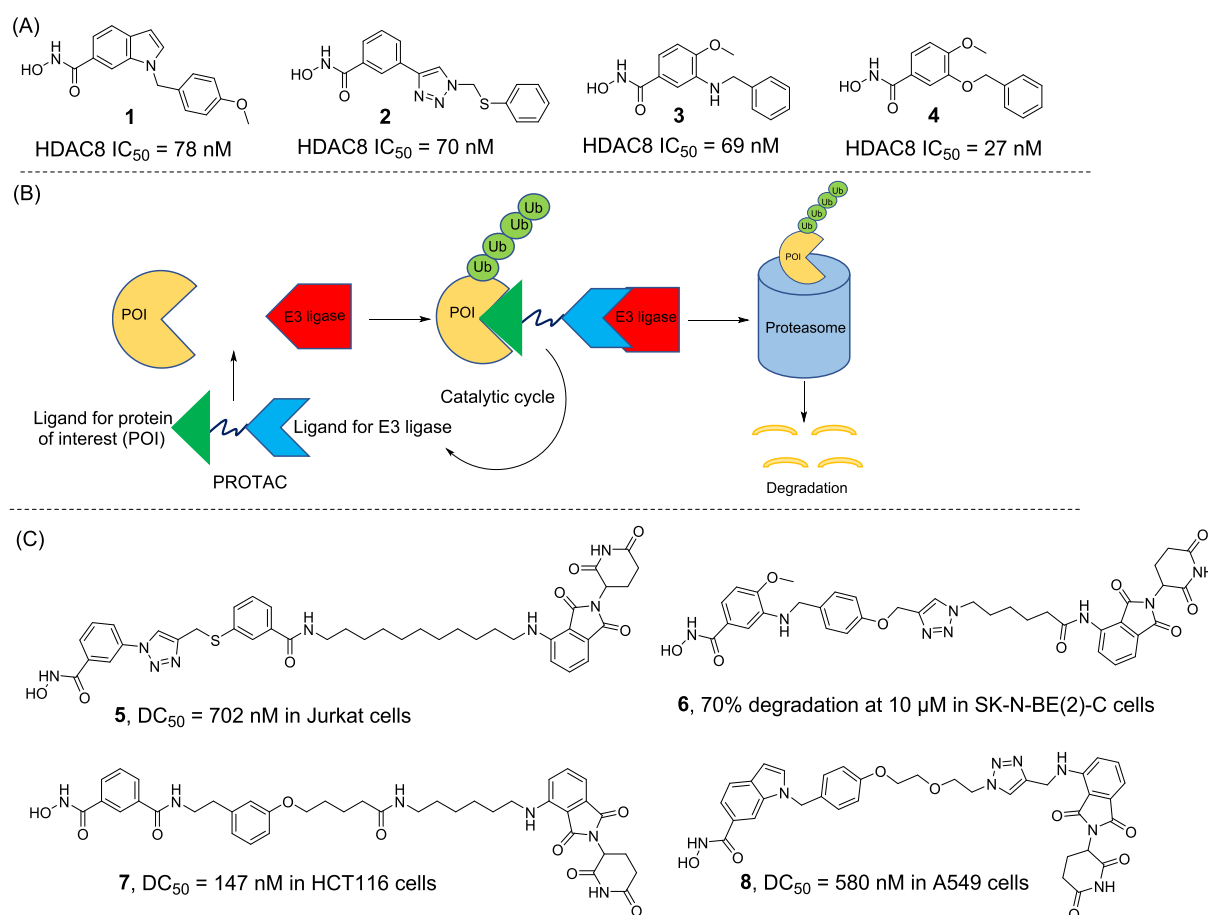


Fig. 1. (A) Representative examples of selective HDAC8 inhibitors. (B) The schematic representation of the PROTAC mode of action. PROTAC binds to both the Protein of Interest (POI) and an E3 ligase, thus enabling POI ubiquitination and proteasomal degradation. (C) Reported HDAC8 PROTACs from literature [44–47].

relationships for HDAC8 PROTACs further in order to achieve PROTACs with improved potency and duration of action.

In this study, we report a novel series of HDAC8 PROTACs by tethering HDAC8 inhibitors to the CRBN recruiter pomalidomide. We identified a potent HDAC8 degradation inducer (CT-4) in both MDA-MB-231 cells and Jurkat cells. A wound healing assay was performed to demonstrate that CT-4 inhibited the migration of MDA-MB-231 cells. Furthermore, growth inhibition was assessed by the MTS in Jurkat cells, which demonstrated potent inhibition of cell viability. Subsequently, apoptosis-induction in Jurkat cells was investigated by the caspase 3/7 activity assay and a flow cytometry assay. Overall, we demonstrate here *in vitro* experimental evidence that CT-4 can be used as a biological tool to investigate the roles of HDAC8 cancer cells. Moreover, it provides potential therapeutic concept for the treatment of HDAC8-related cancers as well.

2. Results and discussion

2.1. Design, synthesis and characterization of HDAC8 PROTACs

Development of HDAC8-selective PROTACs starts from inhibitors that bind selectively to this respective HDAC. Compound 4 (Fig. 1A) shows potent HDAC8 inhibition with lower nanomolar IC₅₀ and has not been used for PROTAC design before [21]. Molecular modeling studies of compound 4 in HDAC8 provided docking poses as depicted in Fig. 2A in which the hydroxamic acid coordinates with the zinc ion and the phenyl group occupies the sub-pocket of HDAC8. This indicates that the phenyl group of compound 4 projects out of the active site and is solvent-exposed, which indicates that attachment of linkers might be tolerated in this position (Fig. 2A). Currently, cereblon (CRBN) recruiters have been widely used for PROTAC development and have more favorable drug-likeness than VHL E3 ligase recruiters [48].

Pomalidomide (9) is a CRBN recruiter, which is widely used for PROTAC design [49]. The co-crystal complex of compound 9 in CRBN showed that compound 9 occupies the active site of CRBN. It's worth noting that the imide moieties of compound 9 is involved in multiple hydrogen bonding interactions with key CRBN amino acid residues, meanwhile leaving the aromatic amine solvent-exposed (Fig. 2B). This binding mode demonstrates that the aromatic amine group of compound 9 can be employed as a linker attachment position. Based on the binding modes, we designed a novel series of HDAC8 PROTACs by connecting compound 4 and compound 9 via flexible aliphatic linkers of various lengths (Fig. 2C).

A collection of HDAC8-directed PROTACs, denoted CT-1 to CT-4, and the negative control (NC-CT-4) were synthesized using procedures shown in Scheme 1. Methyl 3-hydroxy-4-methoxybenzoate (10) was reacted with compound 11 in the presence of K₂CO₃ to give compound 12 in 80% yield. The *tert*-butyl group of compound 12 was hydrolyzed under acid conditions in TFA/CH₂Cl₂ to give compound 13 in 97% yield. Subsequently, compound 13 was condensed with various mono-Boc-diamines in the presence of HATU and DIPEA, followed by methyl ester hydrolysis under basic condition in NaOH_(aq)/MeOH/THF to afford intermediates 14a-14d in 58% – 70% yield. Intermediates 15a and 15b were synthesized according to previously reported methods [51]. The Boc-protection of 14a-14d was removed under acidic conditions followed by reaction with compound 15a or 15b to yield key intermediates 16a-16e in 13% – 21% yield. Finally, compounds 16a-16e were condensed with *O*-(Tetrahydro-2H-pyran-2-yl)hydroxylamine (NH₂OTHP) using EDCI and HOBt as coupling reagents, followed by THP group deprotection in the presence of 4 N HCl in dioxane to afford the target compounds CT-1, CT-2, CT-3, CT-4, and the negative control NC-CT-4 in 16% – 73% yield. The final products were characterized by ¹H and ¹³C NMR and LC-HRMS. The purity of the final products was verified by high-performance liquid chromatography (HPLC), which

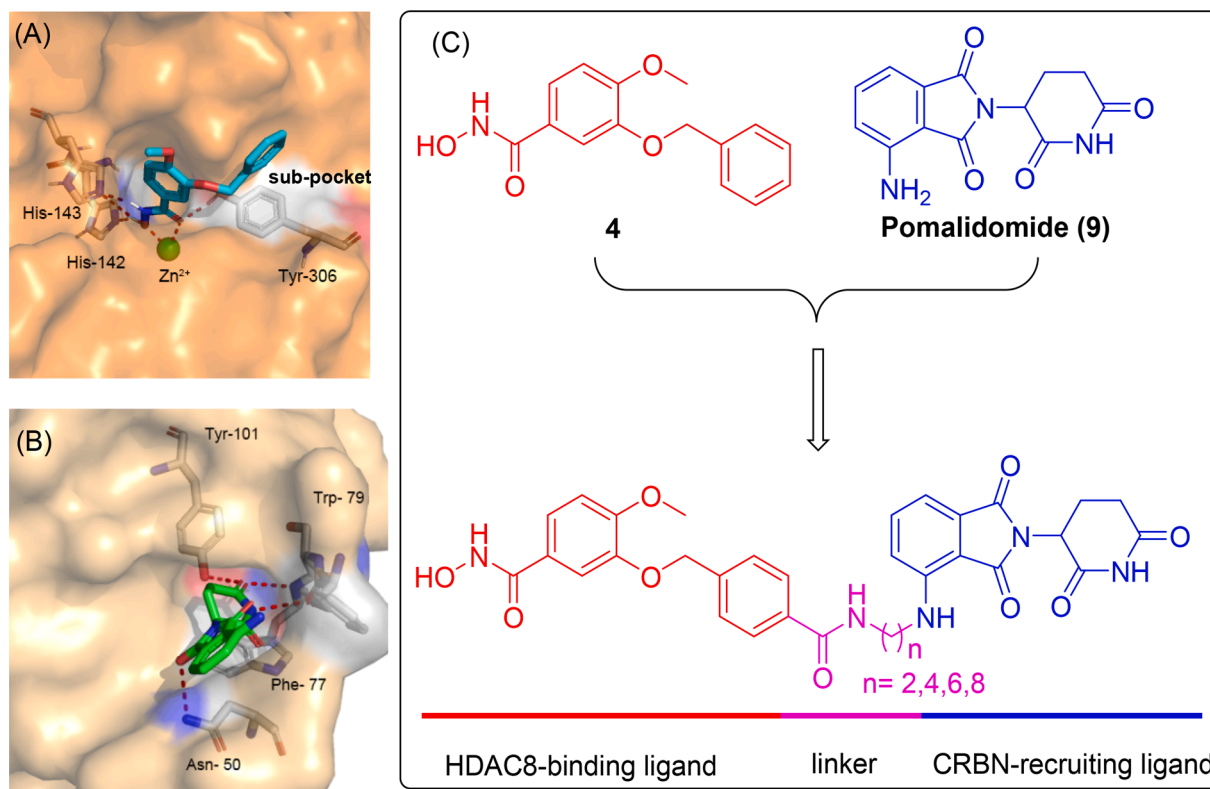
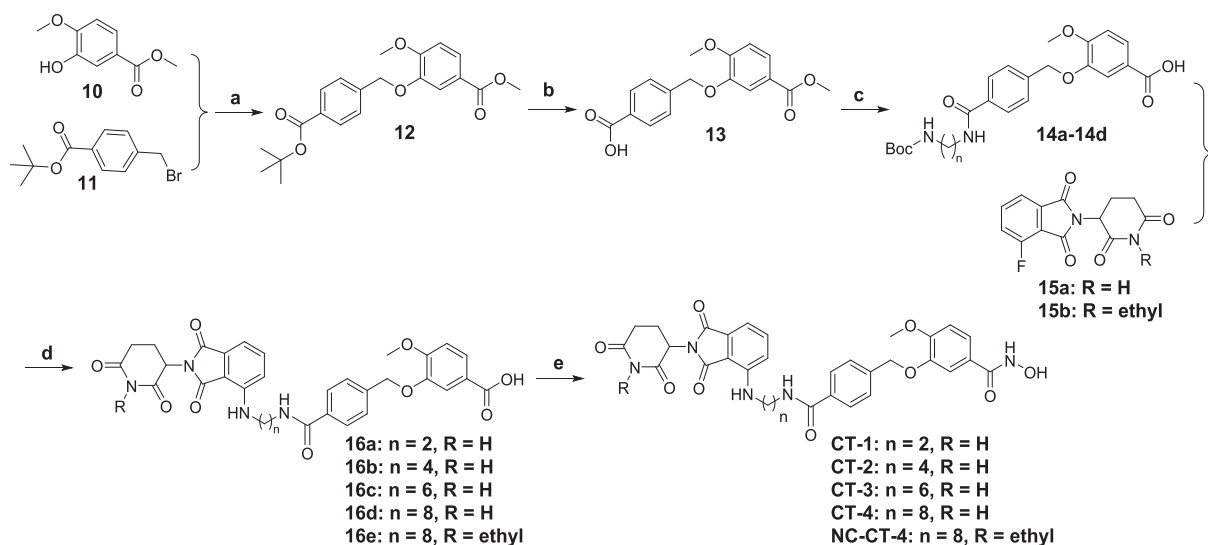


Fig. 2. (A) Proposed binding mode of compound 4 in HDAC8 (PDB Code: 2V5X). The hydrogen bond interactions and zinc ion coordinations were shown as red dash lines. Zinc ion was shown as green sphere. (B) Co-crystal structure of Pomalidomide (9) in CRBN (PDB Code: 4V2Z) [50]. The hydrogen bond interactions were shown as red dash line. (C) Conceptual design of HDAC8 PROTACs. (For interpretation of the references to colour in this figure legend, the reader is referred to the web version of this article.)



Scheme 1. The synthetic route of CT-1, CT-2, CT-3, CT-4, and NC-CT-4. Reagents and conditions: a) K_2CO_3 , DMF, rt; b) TFA/DCM (v/v = 1:2), rt; c) (1) mono-Boc-diamines, HATU, DIPEA, DMF, rt; (2) 1 N NaOH_(aq), THF/MeOH, reflux; d) (1) TFA/DCM (v/v = 1:1), rt; (2) DIPEA, **15a** or **15b**, DMSO, 130°C; e) NH_2OTHP , EDCI, HOBT, DMF, rt; (2) 4 N HCl in dioxane, THF, rt.

demonstrated a purity of at least 95%.

The capacity of PROTACs **CT-1** to **CT-4** to induce HDAC8 degradation was evaluated in triple-negative breast cancer MDA-MB-231 cells. Towards this aim, MDA-MB-231 cells were treated with **CT-1**, **CT-2**, **CT-3**, and **CT-4** at concentrations of 1 μ M and 10 μ M for 24 h and the levels of HDAC8 expression were analyzed using western blot (Fig. 3, Table 1). The degradation percentage was calculated as the percentage of reduction of HDAC8 levels compared to the vehicle control group. All degradation inducers significantly reduced the intracellular level of HDAC8 at both concentrations. At concentration of 10 μ M, the degradation inducers decreased the HDAC8 levels by 44%–93% compared to the vehicle control group. At concentrations around 1 μ M, the degradation was more effective, which may be explained by the “hook effect” in which higher concentrations provide binary complexes of the PROTAC with either HDAC8 or the E3 ligase, instead of the desired target protein-PROTAC-E3 ligase ternary complexes, which will attenuate degradation [52–54]. All the PROTACs provided similar activity in HDAC8 degradation at 1 μ M.

2.2. Characterization of CT-4 as a potent HDAC8 PROTAC

The concentration-dependence of the HDAC8 degradation was investigated for all the PROTACs **CT-1** to **CT-4** in order to determine the DC_{50} and D_{max} values. Towards this aim, MDA-MB-231 cells were treated with a range of concentration of compounds **CT-1**, **CT-2**, **CT-3**, and **CT-4** for 24 h. Changes in the intracellular amount of HDAC8 were determined in response to treatment with various PROTAC concentrations (Fig. 4). The HDAC8 levels were normalized to the vehicle treated control, plotted to the corresponding concentrations and DC_{50} and D_{max} were calculated (Table 2). All degradation inducers reached a $D_{max} > 90\%$ for HDAC8. **CT-4** proved to be the most potent PROTAC with a DC_{50} at about 1.8 nM. Interestingly, shortening the linker length in **CT-1**, **CT-2** and **CT-3** reduced the potency by a factor 10 or more. The “hook effect” appeared at concentrations of 10 μ M, thus indicating that the PROTACs are effective in a reasonably large concentration window.

Because compound **4** showed moderate HDAC6 inhibition [21], we also investigated concentration-dependence of HDAC6 degradation for **CT-1**, **CT-2**, **CT-3**, and **CT-4** in MDA-MB-231 cells. All the PROTACs

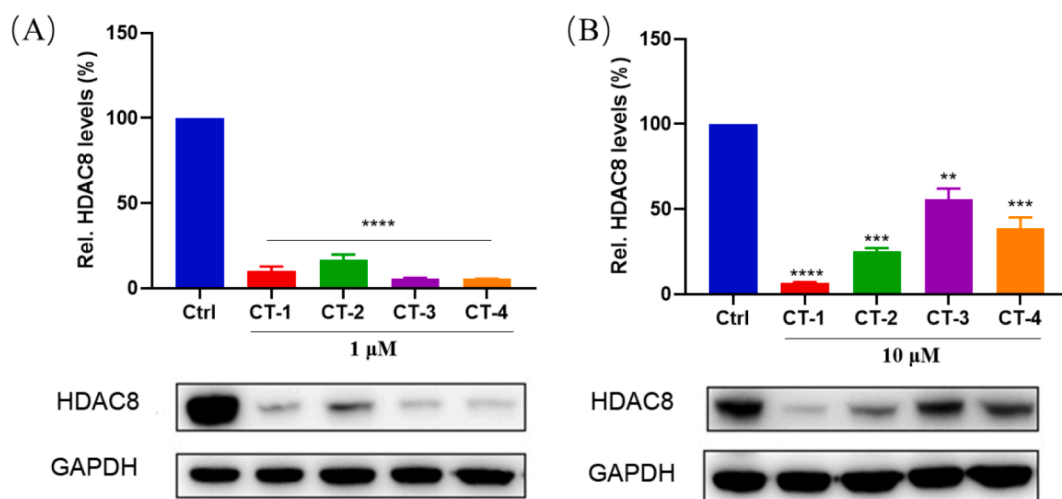
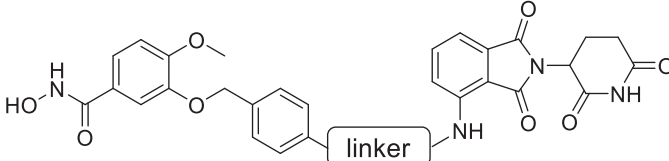
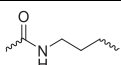
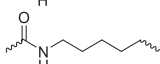
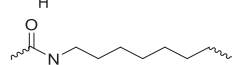
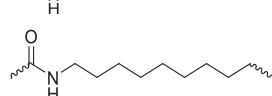


Fig. 3. MDA-MB-231 cells were treated with compounds **CT-1**, **CT-2**, **CT-3**, and **CT-4** at 1 μ M (A) or 10 μ M (B) for 24 h. The HDAC8 levels were detected using western blot. GAPDH was used as loading control. * $P < 0.05$, ** $P < 0.01$, *** $P < 0.001$, and **** $P < 0.0001$ vs vehicle group, one-way analysis of variance (ANOVA). Data are representative of three independent experiments.

Table 1
Reduction of cellular HDAC8 upon treatment with degradation inducers CT-1 to CT-4.



Compounds	Linker	Degradation (%) ^a	
		1 μM	10 μM
CT-1		90 ± 4	93 ± 1
CT-2		83 ± 4	75 ± 3
CT-3		94 ± 1	44 ± 9
CT-4		94 ± 0.1	62 ± 10

^a Degradation percentage is calculated from Fig. 3. Data are shown as [100%-mean (±standard deviation, SD) of relative HDAC8 levels]. Data are representative of three independent experiments.

could reduce the intracellular levels of HDAC6 with a D_{max} of 55%-71%. CT-4 proved also to be the most potent HDAC6 PROTAC in this series with a DC_{50} of 38 nM. The difference in DC_{50} between HDAC8 and HDAC6 is 20-fold for CT-4 (Fig. 4 and Table 2). The 20-fold difference in DC_{50} as well as the lower D_{max} for HDAC6 indicates that a certain level of selectivity between HDAC8 and HDAC6 degradation is reached, but that HDAC6 levels will also be affected upon use of PROTAC CT-4.

We selected CT-4 for further characterization as an HDAC8-directed PROTAC, because it proved to be the most potent HDAC8 PROTAC in this series with over 20-fold selectivity with respect to HDAC6. The selectivity profile of CT-4 was further investigated by the determination of the intracellular level of HDAC1. CT-4 showed no significant effect on the level of HDAC1 (Fig. 5A and Fig. S1A). It is worth noting that CT-4 could dose-dependently increase the levels of both HDAC8 substrate acetylated SMC3 (Ac-SMC3) and HDAC6 substrate acetylated α -tubulin (Ac- α -tubulin), indicating effects on the cellular substrates of HDAC8 and HDAC6 (Fig. 5B and Fig. S1B-C).

HDAC8 degradation by PROTAC CT-4 was analysed further. The kinetics of HDAC8 degradation upon treatment with 0.5 μ M CT-4 showed rapid degradation with a maximum effect of 98% maximal degradation that is reached after 4 h and remained up to 48 h (Fig. 6A). Next, the mechanism of HDAC8 reduction was investigated. We observed significant inhibition of HDAC8 degradation upon pre-treatment with HDAC8 inhibitor 4 or CRBN ligand 9 (Fig. 6B), which indicates that HDAC8 degradation proceeds via ternary complex formation. Also co-treatment with proteasome inhibitor bortezomib inhibited the degradation of HDAC8, thus indicating that HDAC8 degradation is proteasome-dependent. Furthermore, we also synthesized a control compound NC-CT-4 with an ethylated pomalidomide as CRBN ligand (Scheme 1), which is unable to recruit CRBN. NC-CT-4 failed to induce the degradation of HDAC8, suggesting the essential role of CRBN recruitment for degradation. Taken together, these results demonstrate that HDAC8 degradation induced by CT-4 depends on both binding to HDAC8 and CRBN as well as proteasomal activity. Thus, we conclude that CT-4 is an effective and potent HDAC8-directed PROTAC with a moderate selectivity for HDAC8 over HDAC6 (both in D_{50} and D_{max}).

2.3. CT-4 demonstrated limited anti-proliferative activity, but potent anti-migration activity against triple-negative breast cancer MDA-MB-231 cells

After having established CT-4 as potent HDAC8 degradation inducer, its effects on cell proliferation were investigated. The potency of CT-4 on proliferation of MDA-MB-231 cells was evaluated using the MTS assay. PROTAC CT-4 demonstrated a weak anti-proliferative activity, whereas both HDAC8 inhibitor 4 and CRBN ligand 9 did not show obvious anti-proliferative activity against MDA-MB-231, which indicates that HDAC8 contributes little to the proliferation of MDA-MB-231 cells (Fig. S2). In addition, CT-1, CT-2 and CT-3 also showed weak anti-proliferative activities. (Fig. S2).

Because CT-4 shows weak anti-proliferative activity against MDA-MB-231 cells and HDAC8 plays an essential role in the metastasis of MDA-MB-231 cells [25,26], we next investigated the effect of CT-4 on migration of MDA-MB-231 cells. The wound healing assay demonstrated that CT-4 dose-dependently inhibited the migration of MDA-MB-231 cells (Fig. 7). It is worth noting that treatment with 2.5 and 5 μ M PROTAC CT-4 inhibited migration over 40%, while 5 μ M of HDAC8 inhibitor 4 and CRBN ligand 9 had no significant effect on the migration of MDA-MB-231 cells. Based on these results, we can conclude that HDAC8 protein levels are important for migration of MDA-MB-231 cells, whereas inhibition of HDAC8 enzyme activity by 4 or CRBN binding by 9 does not affect migration, which indicates that the HDAC8 protein levels are more important than the HDAC8 lysine deacetylase activity.

2.4. CT-4 induced HDAC8 degradation and cell death in T-cell leukemia Jurkat cells

It has been described that aberrant HDAC8 activities play essential roles in T-cell malignancies and HDAC8 inhibitors have shown anti-proliferative activities against T-cell malignancies [18–20,23]. Therefore, we explored the therapeutic potential of HDAC8 degradation inducer CT-4 against T-cell malignancies. Firstly, we treated T-cell leukemia Jurkat cells with different concentrations of CT-4 and determined the HDAC8 levels (Fig. 8). CT-4 reduced the HDAC8 levels effectively with a DC_{50} value of 4.7 nM and D_{max} of 95%. In comparison the previously reported HDAC8 PROTAC 5 was about 150-fold less potent (DC_{50} = 0.702 μ M) [44]. Although also in this cell line obvious HDAC6 degradation (DC_{50} = 78.5 nM, D_{max} = 76%) was observed, CT-4 still

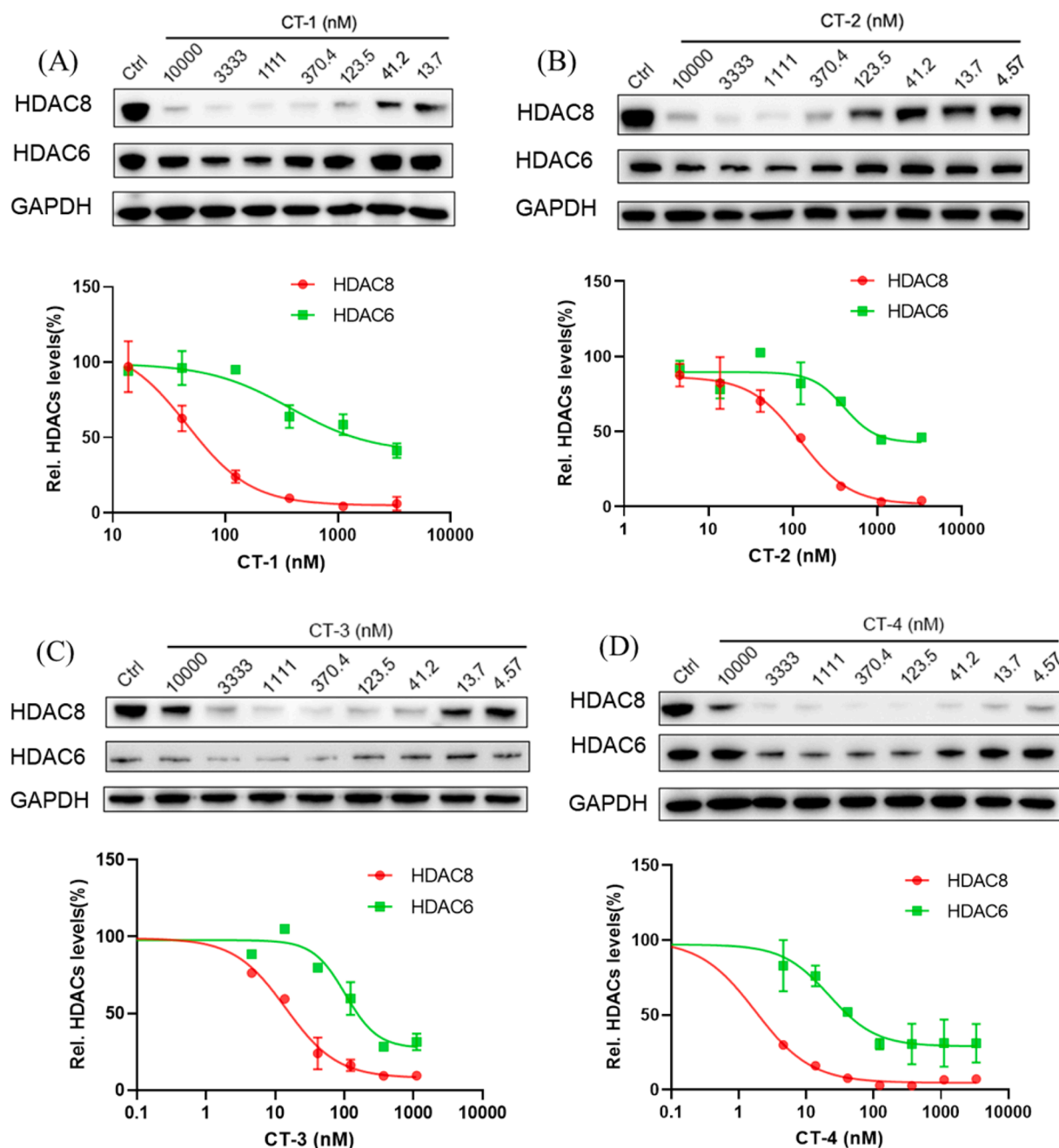


Fig. 4. MDA-MB-231 cells were treated with the indicated concentrations of CT-1 (A), CT-2 (B), CT-3 (C), and CT-4 (D) for 24 h. HDAC8 and HDAC6 levels were determined using western blot. GAPDH was used as loading control. Data were normalized to vehicle (DMSO)-treated group and the dot plot represented as the mean relative expression with \pm SD. Data are representative of at least two independent experiments. Nonlinear fitting was generated by the GraphPad Prism.

Table 2
DC₅₀^a and D_{max}^b Determination^c

Compounds	HDAC8		HDAC6		SI ^d
	DC _{50, 24h} (nM)	D _{max} (%)	DC _{50, 24h} (nM)	D _{max} (%)	
CT-1	53 \pm 8	95 \pm 1	1812 \pm 615	59 \pm 5	34
CT-2	119 \pm 18	96 \pm 1	1114 \pm 241	55 \pm 4	9
CT-3	14 \pm 3	91 \pm 0.4	129 \pm 21	71 \pm 2	9
CT-4	1.8 \pm 0.5	97 \pm 0.6	38 \pm 5	69 \pm 10	21

^a The concentrations at which half-maximal degradation was achieved.

^b The maximum percentage of degradation.

^c DC₅₀ and D_{max} values with \pm SD obtained from nonlinear data in Fig. 4.

^d SI: selectivity index.

retained over 16-fold selectivity (Fig. 8). Moreover, CT-4 did not show significant impact on the level of HDAC1 and HDAC3 (Fig. 8 and Fig. S3). Altogether, this shows that CT-4 has good efficacy and potency to reduce HDAC8 levels and moderate selectivity compared to HDAC6.

Next, we compared the anti-proliferative activity against Jurkat cells between HDAC8 degradation by CT-4 treatment and HDAC8 inhibition by treatment with inhibitor 4. Proliferation of Jurkat cells was investigated by the MTS assay. PROTAC CT-4 demonstrated potent anti-proliferative activity against Jurkat cells with a GI₅₀ value of 2.4 μ M, which was about 10-fold more potent than HDAC8 inhibitor 4 (GI₅₀ = 23 μ M) (Fig. 9), even though CT-4 (HDAC8 IC₅₀ = 1.6 μ M) showed about 9-fold decreased *in vitro* HDAC8 inhibitory activity compared to compound 4 (HDAC8 IC₅₀ = 0.18 μ M) (Fig. S4). In contrast, CRBN ligand 9 showed little or no effect on anti-proliferative activity against Jurkat

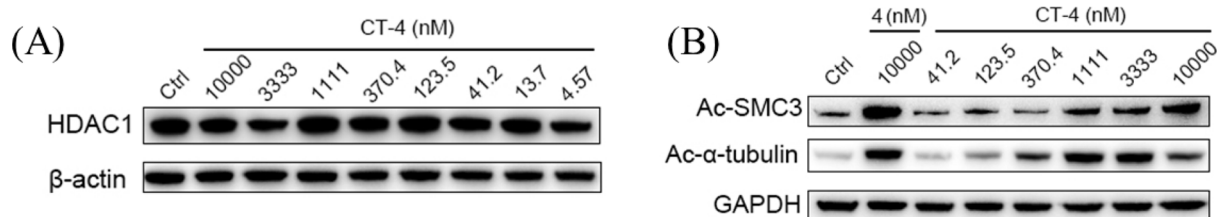


Fig. 5. (A) MDA-MB-231 cells were treated with the indicated concentrations of CT-4 for 24 h. The HDAC1 levels were determined using western blot. β -actin was used as loading control. (B) MDA-MB-231 cells were treated with the indicated concentrations of compound 4 and CT-4 for 24 h. Ac-SMC3 and Ac- α -tubulin levels were determined by western blot. GAPDH was used as loading control. Data are representative of two independent experiments.

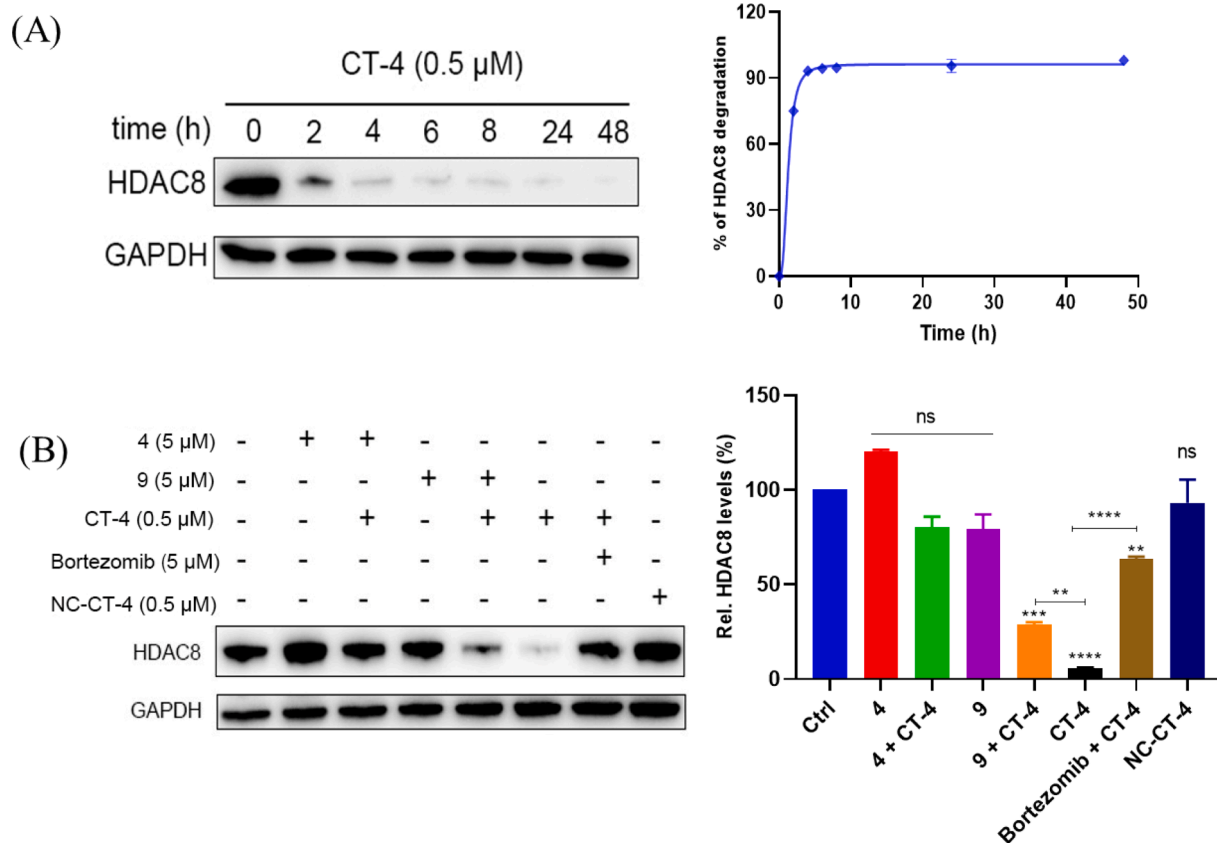


Fig. 6. (A) Time-dependent changes of the HDAC8 levels upon treatment with 0.5 μ M CT-4. GAPDH was used as loading control. (B) Mechanistic investigation of HDAC8 degradation induced by CT-4 in MDA-MB-231 cells. MDA-MB-231 cells were pre-treated with HDAC8 inhibitor 4, CRBN ligand 9, and co-treated with bortezomib, followed by 24 h treatment with CT-4 at 0.5 μ M. MDA-MB-231 cells were treated with NC-CT-4 for 24 h at 0.5 μ M. GAPDH was used as loading control. ns: not significant, * P < 0.05, ** P < 0.01, *** P < 0.001, and **** P < 0.0001 vs vehicle group, one-way analysis of variance (ANOVA). Data are representative of two independent experiments.

cells at $\leq 100 \mu$ M. In addition, co-treatment experiments with compound 4 and 9 provided a GI_{50} value of 34 μ M, indicating that compound 9 can slightly attenuate the cell growth inhibitory activity of compound 4. These results demonstrate that PROTAC CT-4 retains high HDAC8-degrading potency and potently inhibits Jurkat cell viability.

2.5. CT-4 induced apoptosis in Jurkat cells

Because compound 9 and co-treatment with compound 4 and 9 showed weak anti-proliferative activity with GI_{50} values > 33 μ M, we compared the effects of PROTAC CT-4 and inhibitor 4 on cell viability by assays on the induction of apoptosis. Firstly, we performed a caspase 3/7 activity assay, which demonstrated that HDAC8 inhibitor 4 has no significant impact on caspase 3/7 activity, whereas PROTAC CT-4 significantly increased the caspase 3/7 activity in a dose-dependent manner

(Fig. 10A). Next, the apoptosis-inducing ability of PROTAC CT-4 was further evaluated by a flow cytometry assay. Jurkat cells were treated with compound 4 and CT-4 for 48 h, which demonstrated that CT-4 could induce Jurkat cells apoptosis in a dose-dependent manner. Notably, 3 μ M and 10 μ M of CT-4 could induce over 40 % and 60 % Jurkat cells apoptosis, respectively, in contrast to compound 4 that induced only about 8 % apoptosis at 10 μ M (Fig. 10B and 10C). These results indicate that CT-4 has stronger apoptosis-inducing ability than compound 4, which can explain its potent anti-proliferative activity against Jurkat cells (Fig. 9).

3. Conclusion

In the present study, we describe the development of a novel series of HDAC8 PROTACs by linking a known HDAC8 inhibitor to pomalidomide

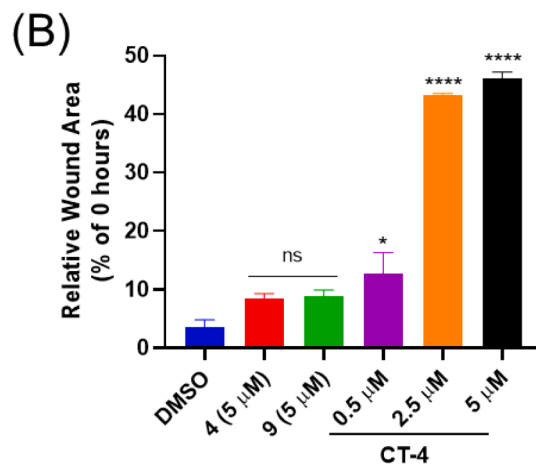
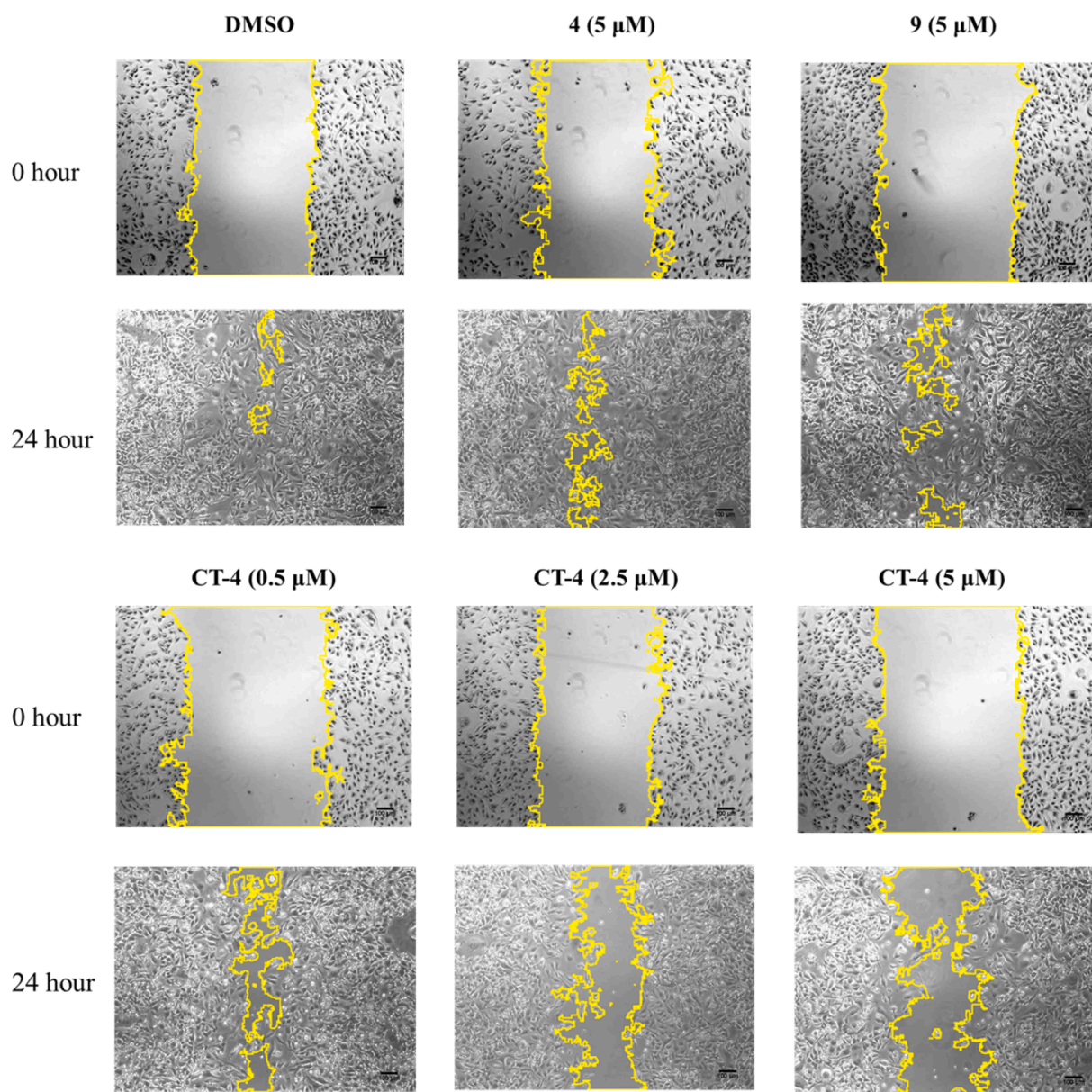


Fig. 7. MDA-MB-231 cells were treated with HDAC8 inhibitor 4, CRBN ligand 9 and PROTAC CT-4 at indicated concentrations for 24 h. Cell migration was measured by wound healing assay (A), and quantitatively analyzed (B). ns: not significant, * $P < 0.05$, ** $P < 0.01$, *** $P < 0.001$, and **** $P < 0.0001$ vs vehicle group, one-way analysis of variance (ANOVA). Values are the mean \pm SD of two independent experiments.

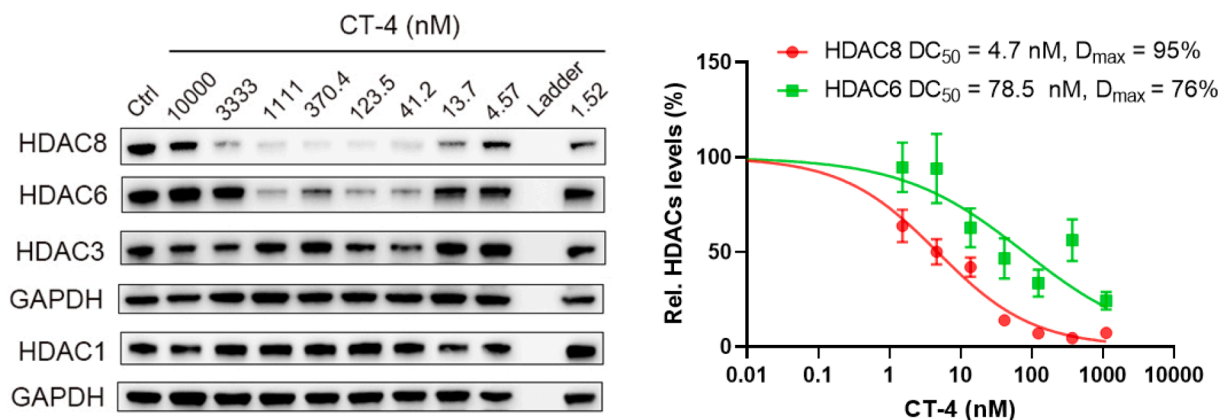


Fig. 8. Jurkat cells were treated with the indicated concentrations of CT-4 for 24 h. HDAC8, HDAC6, HDAC1 and HDAC3 levels were detected by western blot. GAPDH was used as loading control. Data were normalized to vehicle (DMSO)-treated group and the dot plot represented as the mean relative expression with \pm SD. Nonlinear fitting was generated by the GraphPad Prism. Data are representative of at least two independent experiments.

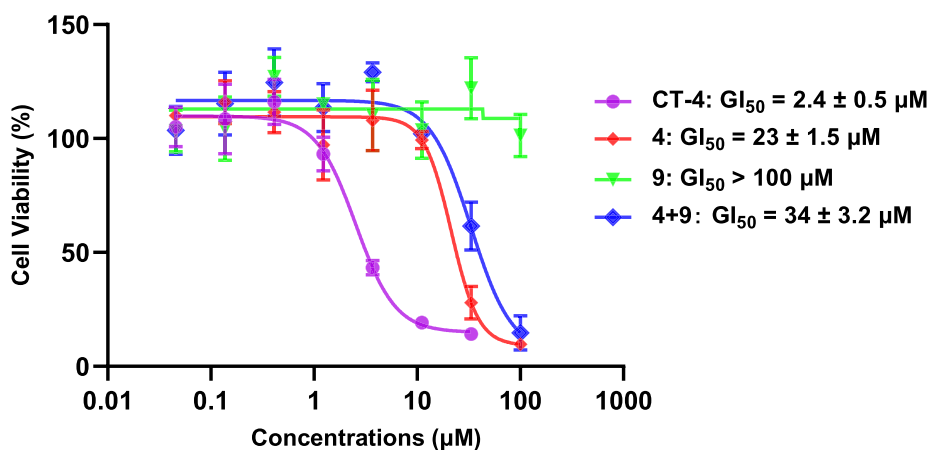


Fig. 9. Jurkat cells were treated with PROTAC CT-4, HDAC8 inhibitor 4, and CRBN ligand 9, and co-treated with 4 and 9 for 72 h. Cell viability was determined by MTS assay. Values are the mean \pm SD of three independent experiments.

via an aliphatic linker of variable length. Among them, CT-4 was identified as a potent HDAC8 PROTAC ($DC_{50} = 1.8$ nM, $D_{max} = 97\%$ in MDA-MB-231 cells, $DC_{50} = 4.7$ nM, $D_{max} = 95\%$ in Jurkat cells). Despite of limited effect on HDAC1 and HDAC3 levels, CT-4 induced HDAC6 degradation in both MDA-MB-231 cells and Jurkat cells albeit with a lower DC_{50} and D_{max} . This indicates that CT-4 has moderate selectivity between HDAC8 and HDAC6, but good selectivity over HDAC1 and HDAC3. Notably, CT-4 effectively inhibited the migration of MDA-MB-231 cells, while it demonstrated limited effect on proliferation, which indicates that HDAC8 contributes little to the proliferation of MDA-MB-231 cells. In Jurkat cells, CT-4 showed potent anti-proliferative activity via induction of apoptosis. In both cell lines the HDAC8 PROTAC performed much better than the HDAC8 inhibitors 4 thus confirming the potential for HDAC8 degradation in oncology. Overall, these results highlight the power and utility of HDAC8 PROTACs not only as new drug modality in HDAC8-directed drug discovery for oncology and other HDAC8-related diseases, but also as molecular tool to investigate the roles of HDAC8 disease models.

4. Experimental section

4.1. Chemistry

Unless otherwise noted, the chemical reagents and solvents were purchased from commercial sources, such as Sigma-Aldrich, BLDpharm, Fluorochem as well as Acros, and were used without further

purification. All reactions were monitored by thin-layer chromatography (TLC) on 0.25 mm silica gel plates (60GF-254). UV light, iodine stain, and ferric chloride were used to visualize the spots. 1H and ^{13}C NMR spectra were recorded on a Bruker DRX spectrometer at 500 MHz, with δ given in parts per million (ppm) and J in hertz (Hz) and using TMS an internal standard. Multiplicity of 1H NMR signals was reported as singlet (s), doublet (d), triplet (t), quartet (q), and multiplet (m). High-resolution mass spectra (HRMS) were recorded using Fourier Transform Mass Spectrometry (FTMS) and Orbitrap XL Hybrid Ion Trap-Orbitrap Mass Spectrometer. Mass spectra were measured on a Waters Investigator Supercritical Fluid Chromatograph with a 3100 MS Detector (ESI). Silica gel was used for column chromatography purification. C18 reverse-phase high performance liquid chromatography (HPLC) analysis was performed to determine the purity of target compounds, and all target compounds achieved a minimum of 95% purity.

4.1.1. Compound 4 was prepared according to the previously reported methods [21].

4.1.1.1 3-(benzyloxy)-N-hydroxy-4-methoxybenzamide (4) The compound was obtained as 0.10 g of a white solid in a yield of 73%. 1H NMR (500 MHz, DMSO- d_6) δ 11.10 (s, 1H), 7.49–7.46 (m, 3H), 7.43–7.39 (m, 3H), 7.37–7.32 (m, 1H), 7.04 (dd, $J = 8.5, 1.1$ Hz, 1H), 5.12 (s, 2H), 3.82 (d, $J = 1.1$ Hz, 3H). ^{13}C NMR (126 MHz, DMSO- d_6) δ 164.33, 151.97, 147.76, 137.37, 128.90, 128.38, 128.31, 125.33, 120.83, 112.41, 111.77, 70.40, 56.19, 56.07. HRMS, calculated 274.1079 for $C_{15}H_{16}NO_4$ $[M + H]^+$, found 274.1071. Purity: 95.6%.

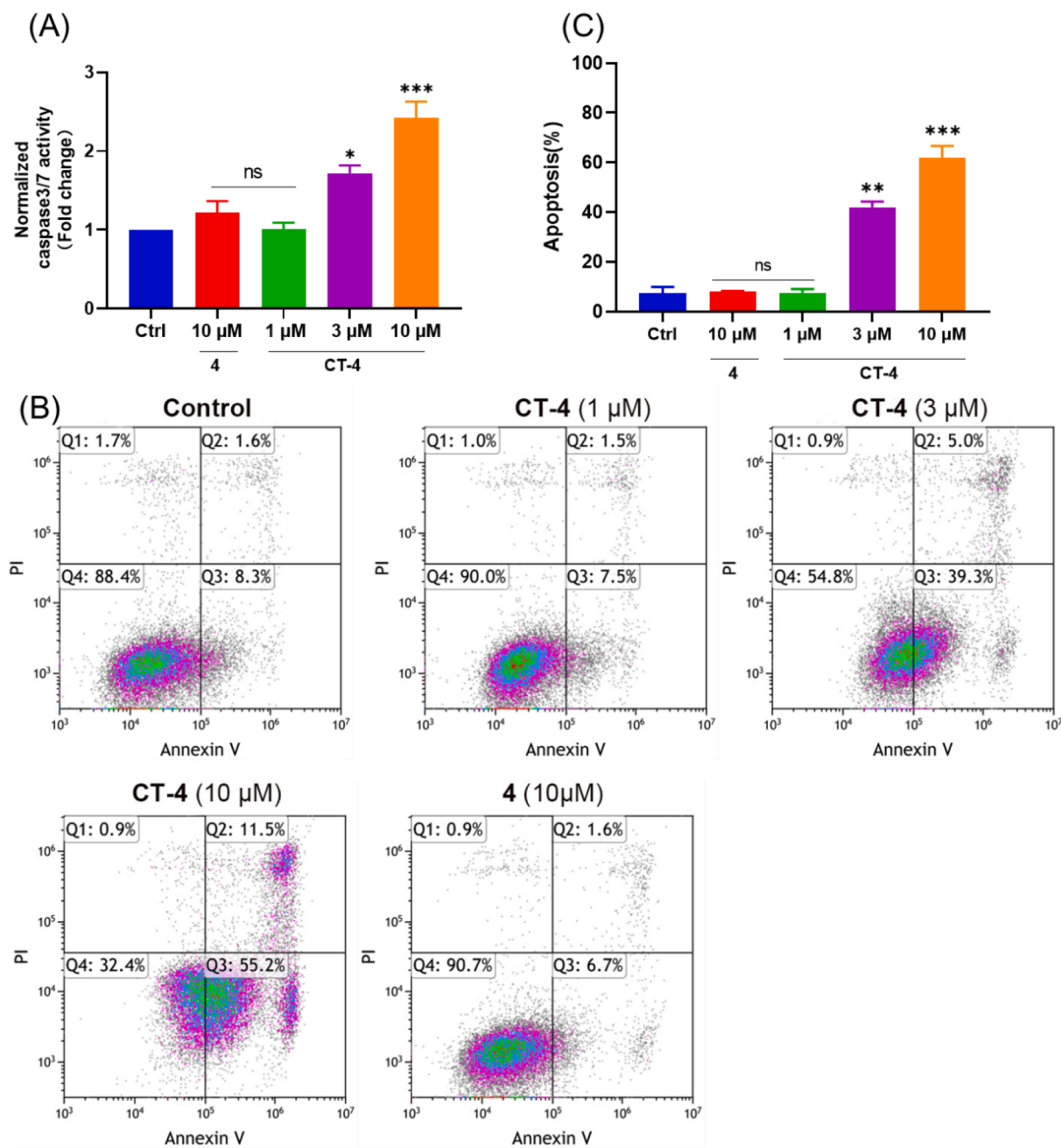


Fig. 10. (A) The caspase 3/7 activity was measured on Jurkat cells treated with the indicated concentrations of HDAC8 inhibitor **4** and PROTAC **CT-4** for 48 h and luminescence was measured after 1 h reagent incubation. All data were normalized to the vehicle control group and shown as mean with SD of three independent experiments. (B) Induction of apoptosis in Jurkat cells after 48 h of treatment. (C) Efficacy of compound **CT-4** at different concentrations to induce apoptosis in Jurkat cells after 48 h of treatment. ns: not significant, * $P < 0.05$, ** $P < 0.01$, *** $P < 0.001$, and **** $P < 0.0001$ vs vehicle group, one-way analysis of variance (ANOVA). Data are shown as mean with SD of two independent experiments.

4.1.2. Methyl 3-((4-(tert-butoxycarbonyl)benzyl)oxy)-4-methoxybenzoate (12)

A mixture of compound **10** (0.36 g, 2.0 mmol) and K_2CO_3 (0.83 g, 6.0 mmol) in 10 mL of dimethylformamide (DMF) was cooled at 0°C, then compound **11** (0.60 g, 2.2 mmol) was added. The resulting mixture was warmed to room temperature and stirred at room temperature for 4 h. Then, the mixture was poured into cold water and extracted with EtOAc. The combined organic layer was washed with brine, dried over $MgSO_4$, filtered, and further purified by column chromatography (Pentane/EtOAc = 10:1 – 4:1) to give 0.60 g of the product as a white solid in a yield of 80%. 1H NMR (500 MHz, $DMSO-d_6$) δ 7.93 (d, $J = 8.0$ Hz, 2H), 7.62 (dd, $J = 8.5, 2.0$ Hz, 1H), 7.58 (d, $J = 8.0$ Hz, 2H), 7.53 (d,

$J = 2.0$ Hz, 1H), 7.12 (d, $J = 8.5$ Hz, 1H), 5.25 (s, 2H), 3.87 (s, 3H), 3.81 (s, 3H), 1.55 (s, 9H). ESI-MS, calculated 395.15 for $C_{21}H_{24}NaO_6$ $[M + Na]^+$, found 395.37.

4.1.3. 4-((2-methoxy-5-(methoxycarbonyl)phenoxy)methyl)benzoic acid (13)

Compound **12** (0.60 g, 1.6 mmol) was dissolved in 4 mL of CH_2Cl_2 (DCM) and the resulting solution was cooled to 0°C, then 2 mL of trifluoroacetic acid (TFA) was added dropwise. The resulting solution was allowed to stir at room temperature for 4 h. Then solvents were removed under reduced pressure to give 0.50 g of the product as a white solid in a yield of 97%. 1H NMR (500 MHz, $DMSO-d_6$) δ 7.98 (d, $J = 8.0$ Hz, 2H),

7.63 (dd, $J = 8.5, 2.0$ Hz, 1H), 7.58 (d, $J = 8.0$ Hz, 2H), 7.55 (d, $J = 2.0$ Hz, 1H), 7.13 (d, $J = 8.5$ Hz, 1H), 5.25 (s, 2H), 3.88 (s, 3H), 3.81 (d, $J = 1.1$ Hz, 3H). ESI-MS, calculated 339.08 for $C_{17}H_{16}NaO_6$ $[M + Na]^+$, found 339.30.

4.1.4. General procedures for synthesis of compounds 14a–14d

Compound **13** (1.0 mmol, 1.0 eq) and HATU (1.2 eq) were dissolved in 5 mL of DMF and the solution was cooled to 0°C followed by the addition of DIPEA (3.0 eq). The resulting solution was stirred at 0°C for 5 mins and respective amines (1.2 eq) were added. The resulting solution was warmed to room temperature and stirred at room temperature for 2 h. Then, the solution was diluted with EtOAc, washed with water, 1 N HCl(aq), saturated NaHCO₃(aq), and brine. The organic layer was dried over MgSO₄, filtered, and concentrated to give intermediate products, which were used without further purification for next step in which the respective intermediate products (1.0 eq) dissolved in 10 mL of THF/H₂O (1:1) after which LiOH (10 eq) was added. The reaction mixtures were stirred at room temperature overnight. The organic solvents were removed under reduced pressure and the pH value of the resulting residues were adjusted to 4–6 by addition of 1 N HCl while cooling on an ice bath. The crude products were collected by filtration.

4.1.4.1. 3-((4-((2-((tert-butoxycarbonyl)amino)ethyl)carbamoyl)benzyl)oxy)-4-methoxybenzoic acid (**14a**). Using the general procedure for the synthesis of compound **14a–14d**, compound **14a** was obtained as 0.27 g of a white solid in a yield of 63%. ¹H NMR (500 MHz, DMSO-*d*₆) δ 12.68 (s, 1H), 8.47 (d, $J = 5.9$ Hz, 1H), 7.86 (d, $J = 8.0$ Hz, 2H), 7.59 (dd, $J = 8.4, 1.9$ Hz, 1H), 7.53 (d, $J = 7.7$ Hz, 3H), 7.09 (d, $J = 8.5$ Hz, 1H), 6.93 (t, $J = 5.8$ Hz, 1H), 5.21 (s, 2H), 3.86 (s, 3H), 3.33–3.27 (m, 2H), 3.11 (q, $J = 6.3$ Hz, 2H), 1.38 (s, 9H). ESI-MS, calculated 467.18 for $C_{23}H_{28}N_2NaO_7$ $[M + Na]^+$, found 467.37.

4.1.4.2. 3-((4-((4-((tert-butoxycarbonyl)amino)butyl)carbamoyl)benzyl)oxy)-4-methoxybenzoic acid (**14b**). Using the general procedure for the synthesis of compound **14a–14d**, compound **14b** was obtained as 0.30 g of an off-white solid in a yield of 64%. ¹H NMR (500 MHz, DMSO-*d*₆) δ 12.68 (s, 1H), 8.46 (t, $J = 5.7$ Hz, 1H), 7.85 (d, $J = 7.9$ Hz, 2H), 7.59 (dd, $J = 8.5, 1.9$ Hz, 1H), 7.53 (dd, $J = 5.2, 3.0$ Hz, 3H), 7.09 (d, $J = 8.5$ Hz, 1H), 6.81 (s, 1H), 5.21 (s, 2H), 3.86 (s, 3H), 3.25 (q, $J = 6.4$ Hz, 2H), 2.97–2.90 (m, 2H), 1.51–1.47 (m, 2H), 1.41–1.22 (m, 11H). ESI-MS, calculated 495.21 for $C_{25}H_{32}N_2NaO_7$ $[M + Na]^+$, found 495.39.

4.1.4.3. 3-((4-((6-((tert-butoxycarbonyl)amino)hexyl)carbamoyl)benzyl)oxy)-4-methoxybenzoic acid (**14c**). Using the general procedure for the synthesis of compound **14a–14d**, compound **14c** was obtained as 0.31 g of a white solid in a yield of 64%. ¹H NMR (500 MHz, DMSO-*d*₆) δ 8.45 (t, $J = 5.5$ Hz, 1H), 7.87–7.84 (m, 2H), 7.59 (dd, $J = 8.5, 1.9$ Hz, 1H), 7.53 (dd, $J = 5.2, 3.3$ Hz, 3H), 7.08 (dd, $J = 8.6, 1.2$ Hz, 1H), 6.79 (t, $J = 5.8$ Hz, 1H), 5.20 (s, 2H), 3.86 (d, $J = 1.2$ Hz, 3H), 3.24 (q, $J = 6.7$ Hz, 2H), 2.90 (q, $J = 6.5$ Hz, 2H), 1.54–1.48 (m, 2H), 1.37–1.34 (m, 11H), 1.33–1.23 (m, 4H). ESI-MS, calculated 523.24 for $C_{27}H_{36}N_2NaO_7$ $[M + Na]^+$, found 523.43.

4.1.4.4. 3-((4-((8-((tert-butoxycarbonyl)amino)octyl)carbamoyl)benzyl)oxy)-4-methoxybenzoic acid (**14d**). Using the general procedure for the synthesis of compound **14a–14d**, compound **14d** was obtained as 0.33 g of a white solid in a yield of 58%. ¹H NMR (500 MHz, DMSO-*d*₆) δ 8.44 (t, $J = 5.7$ Hz, 1H), 7.85 (d, $J = 7.9$ Hz, 2H), 7.59 (dd, $J = 8.4, 1.9$ Hz, 1H), 7.53 (dd, $J = 5.3, 3.2$ Hz, 3H), 7.09 (d, $J = 8.5$ Hz, 1H), 6.76 (t, $J = 5.9$ Hz, 1H), 5.20 (s, 2H), 3.86 (s, 3H), 3.25 (q, $J = 6.7$ Hz, 2H), 2.93–2.85 (m, 2H), 1.56–1.47 (m, 2H), 1.37–1.33 (m, 11H), 1.31–1.22 (m, 8H). ESI-MS, calculated 529.29 for $C_{27}H_{36}N_2O_7$ $[M + H]^+$, found 529.48.

4.1.5. Compounds **15a** and **15b** were prepared according to published methods [51].

4.1.5.1. 2-(2,6-dioxopiperidin-3-yl)-4-fluoroisindoline-1,3-dione (**15a**).

Compound **15a** was obtained as 1.6 g of a white solid in a yield of 58%. ¹H NMR (500 MHz, DMSO-*d*₆) δ 11.17 (s, 1H), 7.96 (td, $J = 8.0, 4.4$ Hz, 1H), 7.80 (d, $J = 7.3$ Hz, 1H), 7.75 (t, $J = 8.9$ Hz, 1H), 5.17 (dd, $J = 13.0, 5.4$ Hz, 1H), 2.90 (ddd, $J = 17.2, 13.9, 5.5$ Hz, 1H), 2.62 (dt, $J = 17.2, 3.4$ Hz, 1H), 2.59–2.52 (m, 1H), 2.07 (dtd, $J = 13.1, 5.4, 2.3$ Hz, 1H). ESI-MS, calculated 277.06 for $C_{13}H_{10}FN_2O_4$ $[M + H]^+$, found 277.33.

4.1.5.2. 2-(1-ethyl-2,6-dioxopiperidin-3-yl)-4-fluoroisindoline-1,3-dione (**15b**).

Compound **15b** was obtained as 0.62 g of a light-yellow solid in a yield of 70%. ¹H NMR (500 MHz, DMSO-*d*₆) δ 7.97 (td, $J = 7.9, 4.4$ Hz, 1H), 7.81 (d, $J = 7.4$ Hz, 1H), 7.76 (t, $J = 8.9$ Hz, 1H), 5.24 (dd, $J = 13.0, 5.5$ Hz, 1H), 3.69 (qt, $J = 9.9, 5.1$ Hz, 2H), 2.98 (ddd, $J = 17.2, 14.0, 5.4$ Hz, 1H), 2.80–2.73 (m, 1H), 2.08 (dtd, $J = 13.1, 5.5, 2.6$ Hz, 1H), 1.03 (t, $J = 7.0$ Hz, 3H). ESI-MS, calculated 305.09 for $C_{15}H_{14}FN_2O_4$ $[M + H]^+$, found 305.34.

4.1.6. General procedures for synthesis of compounds 16a–16e

Intermediates **14a–14d** (0.56 mmol, 1.0 eq) were dissolved in 2 mL of DCM and cooled to 0°C. Then, TFA (2 mL) was added dropwise at 0°C. The resulting solution was warmed to room temperature and stirred at room temperature for 2 h. Then, the solvents were removed under reduced pressure. The obtained crude product was used directly for the next step without further purification. A solution of obtained crude products (0.56 mmol, 1.0 eq), compound **15a** or **15b** (1.0 eq), and DIPEA (4.0 eq) in 5 mL of DMSO was heated at 130°C overnight. The resulting solution was diluted with EtOAc, washed with water, 1 N HCl(aq), and brine. The combined organic layer was dried over MgSO₄, filtered, concentrated, and further purified by column chromatography.

4.1.6.1. 3-((4-((2-((2,6-dioxopiperidin-3-yl)-1,3-dioxoisindolin-4-yl)amino)ethyl)carbamoyl)benzyl)oxy)-4-methoxybenzoic acid (**16a**). Using the general procedures for synthesis of compounds **16a–16e**, compound **14a** and **15a** gave 60 mg of compound **16a** as a yellow solid in a yield of 21%. ¹H NMR (500 MHz, DMSO-*d*₆) δ 11.11 (s, 1H), 8.72 (t, $J = 5.4$ Hz, 1H), 7.86 (d, $J = 7.9$ Hz, 2H), 7.59 (t, $J = 7.4$ Hz, 2H), 7.54 (d, $J = 8.6$ Hz, 3H), 7.27 (d, $J = 8.6$ Hz, 1H), 7.10 (d, $J = 8.5$ Hz, 1H), 7.03 (d, $J = 7.1$ Hz, 1H), 6.87 (s, 1H), 5.21 (s, 2H), 5.06 (dd, $J = 12.8, 5.4$ Hz, 1H), 3.86 (s, 3H), 3.56–3.45 (m, 4H), 2.89 (td, $J = 17.0, 15.4, 5.3$ Hz, 1H), 2.63–2.54 (m, 2H), 2.03 (dd, $J = 12.6, 6.4$ Hz, 1H).

4.1.6.2. 3-((4-((4-((2,6-dioxopiperidin-3-yl)-1,3-dioxoisindolin-4-yl)amino)butyl)carbamoyl)benzyl)oxy)-4-methoxybenzoic acid (**16b**). Using the general procedures for synthesis of compounds **16a–16e**, compound **14b** and **15a** gave 50 mg of compound **16b** as a yellow solid in a yield of 15%. ¹H NMR (500 MHz, DMSO-*d*₆) δ 12.68 (s, 1H), 11.11 (s, 1H), 8.51 (t, $J = 5.7$ Hz, 1H), 7.89–7.83 (m, 2H), 7.61–7.54 (m, 2H), 7.53 (dd, $J = 5.1, 3.0$ Hz, 3H), 7.11 (dd, $J = 14.0, 8.6$ Hz, 2H), 7.02 (d, $J = 7.0$ Hz, 1H), 6.60 (t, $J = 6.0$ Hz, 1H), 5.21 (s, 2H), 5.06 (dd, $J = 12.8, 5.5$ Hz, 1H), 3.86 (s, 3H), 3.32–3.30 (m, 4H), 2.89 (ddd, $J = 17.0, 13.9, 5.5$ Hz, 1H), 2.65–2.57 (m, 1H), 2.08–1.98 (m, 1H), 1.68–1.56 (m, 4H).

4.1.6.3. 3-((4-((6-((2,6-dioxopiperidin-3-yl)-1,3-dioxoisindolin-4-yl)amino)hexyl)carbamoyl)benzyl)oxy)-4-methoxybenzoic acid (**16c**).

Using general procedures for synthesis of compounds **16a–16e**, compound **14c** and **15a** gave 75 mg of compound **16c** as a yellow solid in a yield of 20%. ¹H NMR (500 MHz, DMSO-*d*₆) δ 12.70 (s, 1H), 11.11 (s, 1H), 8.46 (t, $J = 5.7$ Hz, 1H), 7.85 (d, $J = 7.9$ Hz, 2H), 7.62–7.55 (m, 2H), 7.52 (d, $J = 7.4$ Hz, 3H), 7.09 (dd, $J = 8.6, 2.0$ Hz, 2H), 7.02 (d, $J = 7.1$ Hz, 1H), 6.55 (t, $J = 5.8$ Hz, 1H), 5.20 (s, 2H), 5.06 (dd, $J = 12.7, 5.4$ Hz, 1H), 3.86 (s, 3H), 3.31–3.24 (m, 4H), 2.94–2.83 (m, 1H), 2.61–2.57 (m, 1H), 2.06–2.00 (m, 1H), 1.61–1.51 (m, 4H), 1.38 (d, $J = 6.2$ Hz,

4H).

4.1.6.4. 3-((4-((8-((2-(2,6-dioxopiperidin-3-yl)-1,3-dioxoisindolin-4-yl)amino)octyl)carbamoyl)benzyl)oxy)-4-methoxybenzoic acid (16d).

Using the general procedures for synthesis of compounds **16a-16e**, compound **14d** and **15a** gave 70 mg of compound **16d** as a yellow solid in a yield of 17%. ¹H NMR (500 MHz, DMSO-*d*₆) δ 12.67 (s, 1H), 11.10 (s, 1H), 8.44 (t, *J* = 5.8 Hz, 1H), 7.85 (d, *J* = 8.0 Hz, 2H), 7.62–7.56 (m, 2H), 7.52 (d, *J* = 7.3 Hz, 3H), 7.09 (d, *J* = 8.5 Hz, 2H), 7.02 (d, *J* = 7.0 Hz, 1H), 6.53 (t, *J* = 6.0 Hz, 1H), 5.20 (s, 2H), 5.06 (dd, *J* = 12.7, 5.4 Hz, 1H), 3.86 (s, 3H), 3.33–3.21 (m, 4H), 2.89 (td, *J* = 16.2, 14.0, 5.4 Hz, 1H), 2.64–2.51 (m, 2H), 2.09–1.99 (m, 1H), 1.63–1.47 (m, 4H), 1.32 (s, 8H).

4.1.6.5. 3-((4-((8-((2-(1-ethyl-2,6-dioxopiperidin-3-yl)-1,3-dioxoisindolin-4-yl)amino)octyl)carbamoyl)benzyl)oxy)-4-methoxybenzoic acid (16e).

Using the general procedures for synthesis of compounds **16a-16e**, compound **14d** and **15b** gave 60 mg of compound **16e** as a yellow solid in a yield of 13%. ¹H NMR (500 MHz, DMSO-*d*₆) δ 8.44 (t, *J* = 5.6 Hz, 1H), 7.85 (d, *J* = 8.2 Hz, 2H), 7.62–7.56 (m, 2H), 7.55–7.50 (m, 3H), 7.10 (dd, *J* = 8.6, 2.4 Hz, 2H), 7.03 (d, *J* = 7.0 Hz, 1H), 6.55 (s, 1H), 5.20 (s, 2H), 5.13 (dd, *J* = 13.0, 5.4 Hz, 1H), 3.86 (s, 3H), 3.69 (dt, *J* = 8.8, 6.1 Hz, 2H), 3.27 (dt, *J* = 20.2, 6.2 Hz, 4H), 3.03–2.91 (m, 1H), 2.74 (d, *J* = 16.9 Hz, 1H), 2.04 (d, *J* = 12.6 Hz, 1H), 1.57 (d, *J* = 7.3 Hz, 2H), 1.56–1.49 (m, 2H), 1.32 (s, 8H), 1.02 (t, *J* = 7.0 Hz, 3H).

4.1.7. General procedures for synthesis of compounds CT-1, CT-2, CT-3, CT-4, and NC-CT-4

Respective carboxylic acids (0.083 mmol, 1.0 eq), EDCI (1.2 eq), and HOBT (1.2 eq) were dissolved in 5 mL of DMF at 0°C and stirred at 0°C for 10 mins. Then, NH₂OTHP (1.2 eq) was added. The resulting solution was warmed to room temperature and stirred at room temperature overnight. The solution was diluted with EtOAc, washed with water, saturated NaHCO_{3(aq)}, 1 N HCl_(aq), and brine. The organic layer was dried over MgSO₄, filtered, and concentrated to give a yellow solid. The yellow solid was dissolved in 2 mL of tetrahydrofuran (THF) followed by addition of 1.0 mL 4 N HCl in dioxane. The resulting mixture was stirred at room temperature for 1 h. The desired compound was collected by filtration.

4.1.7.1. 3-((4-((2-((2-(2,6-dioxopiperidin-3-yl)-1,3-dioxoisindolin-4-yl)amino)ethyl)carbamoyl)benzyl)oxy)-N-hydroxy-4-methoxybenzamide (CT-1).

Using the general procedures for synthesis of compounds **CT-1, CT-2, CT-3, CT-4, and NC-CT-4**, compound **16a** gave 13 mg of **CT-1** as a yellow solid in a yield of 26%. ¹H NMR (500 MHz, DMSO-*d*₆) δ 11.11 (s, 1H), 11.09 (s, 1H), 8.73 (t, *J* = 5.4 Hz, 1H), 7.86 (d, *J* = 7.9 Hz, 2H), 7.62–7.57 (m, 1H), 7.54 (d, *J* = 7.9 Hz, 2H), 7.46 (d, *J* = 2.0 Hz, 1H), 7.41 (dt, *J* = 8.5, 1.6 Hz, 1H), 7.27 (d, *J* = 8.6 Hz, 1H), 7.04 (t, *J* = 7.9 Hz, 2H), 6.87 (s, 1H), 5.19 (s, 2H), 5.07 (dd, *J* = 12.8, 5.4 Hz, 1H), 3.83 (s, 3H), 3.52 (d, *J* = 6.4 Hz, 2H), 3.47 (q, *J* = 5.5 Hz, 2H), 2.89 (ddd, *J* = 17.1, 13.6, 5.4 Hz, 1H), 2.63–2.51 (m, 2H), 2.02 (ddd, *J* = 14.1, 6.5, 3.5 Hz, 1H). ¹³C NMR (126 MHz, DMSO-*d*₆) δ 173.31, 170.59, 169.18, 167.78, 167.03, 164.27, 151.98, 147.58, 146.82, 140.62, 136.74, 136.63, 134.31, 132.71, 127.88, 127.76, 125.33, 120.95, 117.68, 112.55, 111.80, 111.01, 109.76, 69.91, 56.22, 48.98, 41.77, 39.22, 31.45, 22.63. HRMS, calculated 616.2043 for C₃₁H₃₀N₅O₉ [M + H]⁺, found 616.2037. Purity: 97.1%.

4.1.7.2. 3-((4-((4-((2-(2,6-dioxopiperidin-3-yl)-1,3-dioxoisindolin-4-yl)amino)butyl)carbamoyl)benzyl)oxy)-N-hydroxy-4-methoxybenzamide (CT-2).

Using the general procedures for synthesis of compounds **CT-1, CT-2, CT-3, CT-4, and NC-CT-4**, compound **16b** gave 7 mg of **CT-2** as a yellow solid in a yield of 16%. ¹H NMR (500 MHz, DMSO-*d*₆) δ 11.10 (s, 1H), 8.52 (t, *J* = 5.7 Hz, 1H), 7.86 (d, *J* = 7.9 Hz, 2H), 7.57 (t, *J* = 7.8 Hz, 1H), 7.52 (d, *J* = 7.9 Hz, 2H), 7.46 (d, *J* = 2.0 Hz, 1H), 7.40 (d, *J* = 8.4

Hz, 1H), 7.12 (d, *J* = 8.7 Hz, 1H), 7.03 (dd, *J* = 14.8, 7.7 Hz, 2H), 6.59 (s, 1H), 5.19 (s, 2H), 5.06 (dd, *J* = 12.7, 5.4 Hz, 1H), 3.83 (s, 3H), 3.37–3.29 (m, 4H), 2.89 (td, *J* = 17.8, 15.6, 5.4 Hz, 1H), 2.63–2.51 (m, 2H), 2.06–2.00 (m, 1H), 1.62 (s, 4H). ¹³C NMR (126 MHz, DMSO-*d*₆) δ 173.31, 170.60, 169.39, 167.78, 166.36, 164.25, 151.97, 147.58, 146.86, 140.40, 136.80, 136.67, 134.64, 132.68, 127.84, 127.69, 125.32, 125.32, 120.96, 117.73, 112.61, 111.81, 110.87, 109.47, 69.89, 56.12, 48.99, 42.01, 39.28, 31.45, 27.03, 26.72, 22.62. HRMS, calculated 644.2356 for C₃₃H₃₄N₅O₉ [M + H]⁺, found 644.2354. Purity: 95.4%.

4.1.7.3. 3-((4-((6-((2-(2,6-dioxopiperidin-3-yl)-1,3-dioxoisindolin-4-yl)amino)hexyl)carbamoyl)benzyl)oxy)-N-hydroxy-4-methoxybenzamide (CT-3).

Using the general procedures for synthesis of compounds **CT-1, CT-2, CT-3, CT-4, and NC-CT-4**, compound **16c** gave 30 mg of **CT-3** as a yellow solid in a yield of 50%. ¹H NMR (500 MHz, DMSO-*d*₆) δ 11.11 (s, 1H), 11.08 (s, 1H), 8.46 (t, *J* = 5.5 Hz, 1H), 7.85 (d, *J* = 7.9 Hz, 2H), 7.58 (t, *J* = 7.8 Hz, 1H), 7.52 (d, *J* = 8.0 Hz, 2H), 7.45 (d, *J* = 2.0 Hz, 1H), 7.40 (dd, *J* = 8.6, 2.0 Hz, 1H), 7.10 (d, *J* = 8.6 Hz, 1H), 7.04 (dd, *J* = 13.2, 7.7 Hz, 2H), 6.56 (s, 1H), 5.18 (s, 2H), 5.06 (dd, *J* = 12.8, 5.5 Hz, 1H), 3.83 (s, 3H), 3.33–3.24 (m, 4H), 2.94–2.83 (m, 1H), 2.62–2.56 (m, 1H), 2.57–2.51 (m, 1H), 2.06–2.00 (m, 1H), 1.63–1.51 (m, 4H), 1.38 (s, 4H). ¹³C NMR (126 MHz, DMSO-*d*₆) δ 173.31, 170.60, 169.41, 167.78, 166.29, 164.24, 151.96, 147.57, 146.88, 140.35, 136.80, 134.69, 132.66, 127.84, 127.69, 125.31, 120.97, 117.65, 112.54, 111.81, 110.84, 109.46, 69.89, 56.23, 48.99, 42.25, 31.45, 29.54, 29.11, 26.68, 26.55, 22.62. HRMS, calculated 672.2670 for C₃₅H₃₈N₅O₉ [M + H]⁺, found 672.2667. Purity: 96.0%.

4.1.7.4. 3-((4-((8-((2-(2,6-dioxopiperidin-3-yl)-1,3-dioxoisindolin-4-yl)amino)octyl)carbamoyl)benzyl)oxy)-N-hydroxy-4-methoxybenzamide (CT-4).

Using the general procedures for synthesis of compounds **CT-1, CT-2, CT-3, CT-4, and NC-CT-4**, compound **16d** gave 45 mg of **CT-4** as a yellow solid in a yield of 73%. ¹H NMR (500 MHz, DMSO-*d*₆) δ 11.11 (s, 1H), 11.08 (s, 1H), 8.92 (s, 1H), 8.45 (t, *J* = 5.7 Hz, 1H), 7.85 (d, *J* = 7.8 Hz, 2H), 7.58 (t, *J* = 7.9 Hz, 1H), 7.52 (d, *J* = 7.8 Hz, 2H), 7.45 (d, *J* = 1.9 Hz, 1H), 7.44–7.37 (m, 1H), 7.09 (d, *J* = 8.5 Hz, 1H), 7.04 (dd, *J* = 13.2, 7.7 Hz, 2H), 6.54 (s, 1H), 5.18 (s, 2H), 5.06 (dd, *J* = 12.8, 5.4 Hz, 1H), 3.83 (s, 3H), 3.32–3.23 (m, 4H), 2.94–2.83 (m, 1H), 2.64–2.51 (m, 2H), 2.03 (d, *J* = 13.8 Hz, 1H), 1.58–1.53 (m, 4H), 1.32 (s, 8H). ¹³C NMR (126 MHz, DMSO-*d*₆) δ 173.30, 170.59, 169.42, 167.78, 166.26, 164.30, 151.98, 147.59, 146.90, 140.34, 136.80, 134.72, 132.66, 127.81, 127.75, 127.68, 125.33, 120.94, 117.65, 112.53, 111.81, 110.85, 109.45, 109.45, 69.91, 56.23, 49.00, 42.29, 31.45, 29.58, 29.22, 29.18, 26.94, 26.77, 22.64. HRMS, calculated 700.2982 for C₃₇H₄₂N₅O₉ [M + H]⁺, found 700.2979. Purity: 95.6%.

4.1.7.5. 3-((4-((8-((2-(1-ethyl-2,6-dioxopiperidin-3-yl)-1,3-dioxoisindolin-4-yl)amino)octyl)carbamoyl)benzyl)oxy)-N-hydroxy-4-methoxybenzamide (NC-CT-4).

Using the general procedures for synthesis of compounds **CT-1, CT-2, CT-3, CT-4, and NC-CT-4**, compound **16e** gave 30 mg of **NC-CT-4** as a yellow solid in a yield of 56%. ¹H NMR (500 MHz, DMSO-*d*₆) δ 11.07 (s, 1H), 8.44 (t, *J* = 5.7 Hz, 1H), 7.85 (d, *J* = 8.1 Hz, 2H), 7.59 (t, *J* = 7.8 Hz, 1H), 7.53 (dd, *J* = 8.2, 3.5 Hz, 2H), 7.51–7.37 (m, 2H), 7.13–7.00 (m, 3H), 6.55 (s, 1H), 5.18 (s, 2H), 5.13 (dd, *J* = 13.0, 5.4 Hz, 1H), 3.83 (d, *J* = 3.9 Hz, 3H), 3.69 (dt, *J* = 8.8, 6.4 Hz, 2H), 3.26 (tt, *J* = 12.7, 6.0 Hz, 4H), 2.97 (ddd, *J* = 17.8, 14.0, 5.4 Hz, 1H), 2.78–2.70 (m, 1H), 2.08–2.00 (m, 1H), 1.58 (t, *J* = 6.9 Hz, 2H), 1.51–1.55 (m, 2H), 1.32 (s, 8H), 1.02 (t, *J* = 7.0 Hz, 3H). ¹³C NMR (126 MHz, DMSO-*d*₆) δ 171.85, 169.81, 169.38, 167.74, 166.24, 164.27, 151.98, 147.59, 146.90, 140.33, 136.67, 134.72, 132.65, 127.81, 125.33, 120.93, 117.67, 112.63, 111.81, 110.84, 109.43, 69.93, 56.12, 49.57, 42.30, 35.14, 31.65, 29.55, 29.19, 26.91, 26.76, 21.92, 13.39. HRMS, calculated 728.3296 for C₃₉H₄₆N₅O₉ [M + H]⁺, found 728.3291. Purity: 95.4%.

4.2. Molecular docking

AutoDock was used to model the binding mode of compound **4** in HDAC8 [55,56]. The ligand **4** was prepared and optimized using the AutoDockTools (ADT) v.1.5.7. The crystal structure of HDAC8 (PDB code: 2V5X) was downloaded from PDB (<https://www.rcsb.org/>). Then, all the water molecules in the structure were deleted and polar hydrogens were added using PyMOL, and further optimized by AutoDockTools (ADT) v.1.5.7. AutoDock was utilized for docking with a search box of $50 \times 58 \times 60 \text{ \AA}^3$ to cover the whole active pocket. Other docking parameters were kept to the default values. The docking structure was analyzed by PyMOL (<https://pymol.org/>).

4.3. Cell culture

MDA-MB-231 cell lines were cultured in Dulbecco's Modified Eagle's Medium (DMEM) medium containing 10% (v/v) fetal bovine serum (FBS), 100 U/ml penicillin/streptomycin at 37°C with 5% CO₂ in humidified air. Jurkat cell lines were cultured in RPMI 1640 medium containing 10% (v/v) fetal bovine serum (FBS), 100 U/ml penicillin/streptomycin at 37°C with 5% CO₂ in humidified air.

4.4. Western blot

After treated with DMSO or different concentration of compounds, cells were collected and washed with cold PBS, and subsequently lysed with RIPA lysis buffer supplemented with complete protease inhibitor cocktail, EDTA-free (Roche, Basel, Switzerland) inside. Protein concentrations were determined by a BCA Protein Assay Kit (Thermo Fisher Scientific, USA) according to the manufacturer's protocol. Samples were separated by NuPAGE™ 4–12% Bis-Tris gels (Invitrogen, Carlsbad, Canada), and transferred onto polyvinylidene fluoride (PVDF) membranes. The membranes were blocked at room temperature for 1 h in 0.1% PBST solution containing 5% skimmed milk, and subsequently incubated at 4°C overnight with corresponding primary antibodies in 5% BSA in 0.1% PBST solution. Membranes were washed three times in 0.1% PBST and incubated at room temperature for 1 h with corresponding secondary antibody. The bonds were visualized via ECL chemiluminescent western blot detection.

4.5. Cell viability

MTS assay was used to measure the cell viability. MDA-MB-231 (5000 cells/well) and Jurkat (10000 cells/well) were seeded in 96-well plates in 100 µL complete medium. After overnight seeding, 50 µL of media containing various concentrations of compounds or the vehicle was added to each well. After 72 h of treatment, 20 µL of Cell-Titer 96® AQueous One Solution reagent (Promega, Madison, USA) was added to each well according to manufacturer's protocol. Plates were incubated at 37°C for 1–2 h. The absorbance was determined at a wavelength of 490 nm using a Synergy H1 plate reader (Biotek, Winooski, VT, USA).

4.6. Wound healing assay

MDA-MB-231 cells were seeded in a 6-well plate. After the formation of a complete monolayer, cells were scratched using a yellow tip. After scratching, cells were washed twice with PBS. Then, the cells were treated with compounds dissolved in medium with 3% FBS. Images at different time points (0 and 24 h) were taken on a light microscope. The relative wound area is calculated using Image J software.

4.7. In vitro HDAC8 inhibition assay

Black 96-well flat-bottom microplates were used for the HDAC8 inhibition assay. Human recombinant C-terminal His-tag HDAC8 (BPS

Bioscience, Catalog #50008) was diluted (1 µg/mL) with assay buffer (25 mM Tris-HCl, pH 8.0, 137 mM NaCl, 2.7 mM KCl, 1 mM MgCl₂, 0.01% Triton-X and 1 mg/mL BSA). 40 µL of this HDAC8 enzyme dilution was incubated with 10 µL of different concentrations of inhibitors in 10% DMSO/incubation buffer for 5 min at room temperature. Then 50 µL of the fluorogenic Boc-Lys (trifluoroacetyl)-AMC (20 mM) and the plate was incubated at 37 °C for 30 min. Then, 50 µL of the stop solution (25 mM Tris-HCl (pH 8), 137 mM NaCl, 2.7 mM KCl, 1 mM MgCl₂, 0.01% Triton-X, 6.0 mg/mL trypsin and 200 mM SAHA) was added, and the assay development was allowed to proceed for 20 min at 37°C. Fluorescence was then analyzed with an excitation of 350–360 nm and an emission wavelength of 450–460 nm at a microplate reader. The IC₅₀ values were calculated using nonlinear regression with normalized dose–response fit using Prism GraphPad software.

4.8. Caspase 3/7 activity assay

Jurkat cells were seeded in white-walled 96-well plates (Greiner bio-one, Alphen a/d Rijn, The Netherlands) in 100 µL complete medium and cultured overnight. Then, 50 µL of compounds were added to the plates and incubated for 48 h. The Caspase-Glo 3/7 Reagent (Promega Corporation, Madison, WI, USA) was equilibrated to room temperature, and 150 µL of the reagent was added to each well. After incubation at room temperature for 1 h, the luminescence was collected using a Synergy H1 plate reader (Biotek, Winooski, VT, USA).

4.9. Flow cytometry assay

The cell apoptosis assay was performed using eBioscience™ Annexin V-FITC/PI Apoptosis Detection Kit (Thermo Fisher Scientific, Carlsbad, CA, USA). Jurkat cells (5×10^5) were treated with different concentrations of test compounds for 48 h. Cells were harvested after incubation, washed twice in cold PBS, centrifuged, and resuspended in 1X annexin-binding buffer. According to the manufacturer's instructions, cells were incubated with annexin V and Propidium iodide (PI) sequentially. All samples were analyzed by NovoCyte Quanteon Flow Cytometer (Agilent Technologies, CA, USA). The results were analyzed using Kaluza Analysis software.

Declaration of Competing Interest

The authors declare the following financial interests/personal relationships which may be considered as potential competing interests: Chunlong Zhao, Deng Chen, Fengzhi Suo reports financial support was provided by China Scholarship Council.

Data availability

Data will be made available on request.

Acknowledgements

Chunlong Zhao, Deng Chen and Fengzhi Suo are funded by China Scholarship Council (grant no. 202006220019 for Chunlong Zhao, grant no. 201907720019 for Deng Chen, grant no. 201907040076 for Fengzhi Suo).

Appendix A. Supplementary material

Supplementary data to this article can be found online at <https://doi.org/10.1016/j.bioorg.2023.106546>.

References

- [1] T.C.S. Ho, A.H.Y. Chan, A. Ganesan, Thirty Years of HDAC Inhibitors: 2020 Insight and Hindsight, *J Med Chem* 63 (21) (2020) 12460–12484, <https://doi.org/10.1021/acs.jmedchem.0c00830>.
- [2] K.J. Falkenberg, R.W. Johnstone, Histone deacetylases and their inhibitors in cancer, neurological diseases and immune disorders, *Nat Rev Drug Discov* 13 (9) (2014) 673–691, <https://doi.org/10.1038/nrd4360>.
- [3] S.E. Bates, Epigenetic Therapies for Cancer, *N Engl J Med* 383 (7) (2020) 650–663, <https://doi.org/10.1056/NEJMra1805035>.
- [4] M.J. Bishton, S.J. Harrison, B.P. Martin, N. McLaughlin, C. James, E.C. Josefsson, K.J. Henley, B.T. Kile, H.M. Prince, R.W. Johnstone, Deciphering the molecular and biologic processes that mediate histone deacetylase inhibitor-induced thrombocytopenia, *Blood* 117 (13) (2011) 3658–3668, <https://doi.org/10.1182/blood-2010-11-318055>.
- [5] S. Subramanian, S.E. Bates, J.J. Wright, I. Espinoza-Delgado, R.L. Piekarz, Clinical Toxicities of Histone Deacetylase Inhibitors, *Pharmaceuticals (Basel)* 3 (9) (2010) 2751–2767, <https://doi.org/10.3390/ph3092751>.
- [6] A. Chakrabarti, I. Oehme, O. Witt, G. Oliveira, W. Sippl, C. Romier, R.J. Pierce, M. Jung, HDAC8: a multifaceted target for therapeutic interventions, *Trends Pharmacol Sci* 36 (7) (2015) 481–492, <https://doi.org/10.1016/j.tips.2015.04.013>.
- [7] A. Chakrabarti, J. Melesina, F.R. Kolbinger, I. Oehme, J. Senger, O. Witt, W. Sippl, M. Jung, Targeting histone deacetylase 8 as a therapeutic approach to cancer and neurodegenerative diseases, *Future Med Chem* 8 (13) (2016) 1609–1634.
- [8] J.Y. Kim, H. Cho, J. Yoo, G.W. Kim, Y.H. Jeon, S.W. Lee, S.H. Kwon, Pathological Role of HDAC8, Cancer and Beyond, *Cells* 11 (19) (2022), <https://doi.org/10.3390/cells11193161>.
- [9] M.A. Deardorff, M. Bando, R. Nakato, E. Watrin, T. Itoh, M. Minamoto, K. Saitoh, M. Komata, Y. Katou, D. Clark, K.E. Cole, E. De Baere, C. Decroos, N. Di Donato, S. Ernst, L.J. Francey, Y. Gyftodimou, K. Hirashima, M. Hullings, Y. Ishikawa, C. Jaulin, M. Kaur, T. Kiyono, P.M. Lombardi, L. Magnaghi-Jaulin, G.R. Mortier, N. Nozaki, M.B. Petersen, H. Seimiya, V.M. Siu, Y. Suzuki, K. Takagaki, J.J. Wilde, P.J. Willems, C. Prigent, G. Gillissen-Kaesbach, D.W. Christianson, F.J. Kaiser, L. G. Jackson, T. Hirota, I.D. Krantz, K. Shirahige, HDAC8 mutations in Cornelia de Lange syndrome affect the cohesin acetylation cycle, *Nature* 489 (7415) (2012) 313–317, <https://doi.org/10.1038/nature11316>.
- [10] J. Qi, S. Singh, W.K. Hua, Q. Cai, S.W. Chao, L. Li, H. Liu, Y. Ho, T. McDonald, A. Lin, G. Marcucci, R. Bhatia, W.J. Huang, C.I. Chang, Y.H. Kuo, HDAC8 Inhibition Specifically Targets Inv(16) Acute Myeloid Leukemic Stem Cells by Restoring p53 Acetylation, *Cell Stem Cell* 17 (5) (2015) 597–610, <https://doi.org/10.1016/j.stem.2015.08.004>.
- [11] Y. Kang, H. Nian, P. Rajendran, E. Kim, W.M. Dashwood, J.T. Pinto, L. A. Boardman, S.N. Thibodeau, P.J. Limburg, C.V. Lohr, W.H. Bisson, D.E. Williams, E. Ho, R.H. Dashwood, HDAC8 and STAT3 repress BMF gene activity in colon cancer cells, *Cell Death Dis* 5 (2014) e1476.
- [12] J. Gao, B. Siddoway, Q. Huang, H. Xia, Inactivation of CREB mediated gene transcription by HDAC8 bound protein phosphatase, *Biochem Biophys Res Commun* 379 (1) (2009) 1–5, <https://doi.org/10.1016/j.bbrc.2008.11.135>.
- [13] Y. Qian, J. Zhang, Y.S. Jung, X. Chen, DECI coordinates with HDAC8 to differentially regulate Tap73 and DeltaNp73 expression, *PLoS One* 9 (1) (2014) e84015.
- [14] A. Fontana, I. Cursaro, G. Carullo, S. Gemma, S. Butini, G. Campiani, A Therapeutic Perspective of HDAC8 in Different Diseases: An Overview of Selective Inhibitors, *Int J Mol Sci* 23 (17) (2022), <https://doi.org/10.3390/ijms231710014>.
- [15] S. Banerjee, N. Adhikari, S.A. Amin, T. Jha, Histone deacetylase 8 (HDAC8) and its inhibitors with selectivity to other isoforms: An overview, *Eur J Med Chem* 164 (2019) 214–240, <https://doi.org/10.1016/j.ejmech.2018.12.039>.
- [16] S.A. Amin, N. Adhikari, T. Jha, Structure-activity relationships of HDAC8 inhibitors: Non-hydroxamates as anticancer agents, *Pharmacol Res* 131 (2018) 128–142, <https://doi.org/10.1016/j.phrs.2018.03.001>.
- [17] W. Yan, S. Liu, E. Xu, J. Zhang, Y. Zhang, X. Chen, X. Chen, Histone deacetylase inhibitors suppress mutant p53 transcription via histone deacetylase 8, *Oncogene* 32 (5) (2013) 599–609, <https://doi.org/10.1038/ncr.2012.81>.
- [18] T. Suzuki, Y. Ota, M. Ri, M. Bando, A. Gotoh, Y. Itoh, H. Tsumoto, P.R. Tatum, T. Mizukami, H. Nakagawa, S. Iida, R. Ueda, K. Shirahige, N. Miyata, Rapid discovery of highly potent and selective inhibitors of histone deacetylase 8 using click chemistry to generate candidate libraries, *J Med Chem* 55 (22) (2012) 9562–9575, <https://doi.org/10.1021/jm300837y>.
- [19] S. Balasubramanian, J. Ramos, W. Luo, M. Sirisawad, E. Verner, J.J. Buggy, A novel histone deacetylase 8 (HDAC8)-specific inhibitor PCI-34051 induces apoptosis in T-cell lymphomas, *Leukemia* 22 (5) (2008) 1026–1034, <https://doi.org/10.1038/leu.2008.9>.
- [20] M. Marek, T.B. Shaik, T. Heimburg, A. Chakrabarti, J. Lancelot, E. Ramos-Morales, C. Da Veiga, D. Kalinin, J. Melesina, D. Robaa, K. Schmidt-kunz, T. Suzuki, R. Holl, E. Ennifar, R.J. Pierce, M. Jung, W. Sippl, C. Romier, Characterization of Histone Deacetylase 8 (HDAC8) Selective Inhibition Reveals Specific Active Site Structural and Functional Determinants, *J Med Chem* 61 (22) (2018) 10000–10016, <https://doi.org/10.1021/acs.jmedchem.8b01087>.
- [21] T. Heimburg, F.R. Kolbinger, P. Zeyen, E. Ghazy, D. Herp, K. Schmidt-kunz, J. Melesina, T.B. Shaik, F. Erdmann, M. Schmidt, C. Romier, D. Robaa, O. Witt, I. Oehme, M. Jung, W. Sippl, Structure-Based Design and Biological Characterization of Selective Histone Deacetylase 8 (HDAC8) Inhibitors with Anti-Neuroblastoma Activity, *J Med Chem* 60 (24) (2017) 10188–10204, <https://doi.org/10.1021/acs.jmedchem.7b01447>.
- [22] M.M. Hassan, J. Israelian, N. Nawar, G. Ganda, P. Manaswiyoungkul, Y.S. Raouf, D. Armstrong, A. Sedighi, O.O. Olaoye, F. Erdogan, A.D. Cabral, F. Angeles, R. Altintas, E.D. de Araujo, P.T. Gunning, Characterization of Conformationally Constrained Benzamide Scaffolds for Potent and Selective HDAC8 Targeting, *J Med Chem* 63 (15) (2020) 8634–8648, <https://doi.org/10.1021/acs.jmedchem.0c01025>.
- [23] C. Zhao, J. Zang, Q. Ding, E.S. Inks, W. Xu, C.J. Chou, Y. Zhang, Discovery of meta-sulfamoyl N-hydroxybenzamides as HDAC8 selective inhibitors, *Eur J Med Chem* 150 (2018) 282–291, <https://doi.org/10.1016/j.ejmech.2018.03.002>.
- [24] M. Liao, J. Zhang, G. Wang, L. Wang, J. Liu, L. Ouyang, B. Liu, Small-Molecule Drug Discovery in Triple Negative Breast Cancer: Current Situation and Future Directions, *J Med Chem* 64 (5) (2021) 2382–2418, <https://doi.org/10.1021/acs.jmedchem.0c01180>.
- [25] P. An, F. Chen, Z. Li, Y. Ling, Y. Peng, H. Zhang, J. Li, Z. Chen, H. Wang, HDAC8 promotes the dissemination of breast cancer cells via AKT/GSK-3beta/Snail signals, *Oncogene* 39 (26) (2020) 4956–4969, <https://doi.org/10.1038/s41388-020-1337-x>.
- [26] X. Tang, G. Li, F. Su, Y. Cai, L. Shi, Y. Meng, Z. Liu, J. Sun, M. Wang, M. Qian, Z. Wang, X. Xu, Y.X. Cheng, W.G. Zhu, B. Liu, HDAC8 cooperates with SMAD3/4 complex to suppress SIRT7 and promote cell survival and migration, *Nucleic Acids Res* 48 (6) (2020) 2912–2923, <https://doi.org/10.1093/nar/gkaa039>.
- [27] M. Toure, C.M. Crews, Small-Molecule PROTACs: New Approaches to Protein Degradation, *Angew Chem Int Ed Engl* 55 (6) (2016) 1966–1973, <https://doi.org/10.1002/anie.201507978>.
- [28] M. Bekes, D.R. Langley, C.M. Crews, PROTAC targeted protein degraders: the past is prologue, *Nat Rev Drug Discov* 21 (3) (2022) 181–200, <https://doi.org/10.1038/s41573-021-00371-6>.
- [29] A.C. Lai, C.M. Crews, Induced protein degradation: an emerging drug discovery paradigm, *Nat Rev Drug Discov* 16 (2) (2017) 101–114, <https://doi.org/10.1038/nrd.2016.211>.
- [30] K.T.G. Samarasinghe, C.M. Crews, Targeted protein degradation: A promise for undruggable proteins, *Cell Chem Biol* 28 (7) (2021) 934–951, <https://doi.org/10.1016/j.chembiol.2021.04.011>.
- [31] C. Zhao, F.J. Dekker, Novel Design Strategies to Enhance the Efficiency of Proteolysis Targeting Chimeras, *ACS Pharmacol Transl Sci* 5 (9) (2022) 710–723, <https://doi.org/10.1021/acspstsci.2c00089>.
- [32] D. Sun, J. Zhang, G. Dong, S. He, C. Sheng, Blocking Non-enzymatic Functions by PROTAC-Mediated Targeted Protein Degradation, *J Med Chem* 65 (21) (2022) 14276–14288, <https://doi.org/10.1021/acs.jmedchem.2c01159>.
- [33] Y. Xiong, K.A. Donovan, N.A. Eleuteri, N. Kirmani, H. Yue, A. Razov, N. M. Krupnick, R.P. Nowak, E.S. Fischer, Chemo-proteomics exploration of HDAC degradability by small molecule degraders, *Cell Chem Biol* 28 (10) (2021) 1514–1527, <https://doi.org/10.1016/j.chembiol.2021.07.002>.
- [34] Y. Xiao, J. Wang, L.Y. Zhao, X. Chen, G. Zheng, X. Zhang, D. Liao, Discovery of histone deacetylase 3 (HDAC3)-specific PROTACs, *Chem Commun (Camb)* 56 (68) (2020) 9866–9869, <https://doi.org/10.1039/d0cc03243c>.
- [35] F. Cao, S. de Weerd, D. Chen, M.R.H. Zwinderman, P.E. van der Wouden, F. J. Dekker, Induced protein degradation of histone deacetylases 3 (HDAC3) by proteolysis targeting chimera (PROTAC), *Eur J Med Chem* 208 (2020), 112800, <https://doi.org/10.1016/j.ejmech.2020.112800>.
- [36] H. Wu, K. Yang, Z. Zhang, E.D. Leisten, Z. Li, H. Xie, J. Liu, K.A. Smith, Z. Novakova, C. Barinka, W. Tang, Development of Multifunctional Histone Deacetylase 6 Degraders with Potent Antimyeloma Activity, *J Med Chem* 62 (15) (2019) 7042–7057, <https://doi.org/10.1021/acs.jmedchem.9b00516>.
- [37] L.A.A. Fabian Fischer, LaoiseMurray and Thomas Kurz, Designing HDAC-PROTACs: lessons learned so far, *Future Med Chem* 14(3) (2022) 143–166.
- [38] N. Macabuga, W. Esmieu, P. Breccia, R. Jarvis, W. Blackaby, O. Lazari, L. Urbonas, M. Eznarriaga, R. Williams, A. Strijbosch, R. Van de Bospoort, K. Matthews, C. Clissold, T. Ladduwahetty, H. Vater, P. Heaphy, D.G. Stafford, H.J. Wang, J. E. Mangette, G. McAllister, V. Beaumont, T.F. Vogt, H.A. Wilkinson, E.M. Doherty, C. Dominguez, Developing HDAC4-Selective Protein Degraders To Investigate the Role of HDAC4 in Huntington's Disease Pathology, *J Med Chem* 65 (18) (2022) 12445–12459, <https://doi.org/10.1021/acs.jmedchem.2c01149>.
- [39] J.P. Smalley, I.M. Baker, W.A. Pytel, L.Y. Lin, K.J. Bowman, J.W.R. Schwabe, S. M. Cowley, J.T. Hodgkinson, Optimization of Class I Histone Deacetylase PROTACs Reveals that HDAC1/2 Degradation is Critical to Induce Apoptosis and Cell Arrest in Cancer Cells, *J Med Chem* 65 (7) (2022) 5642–5659, <https://doi.org/10.1021/acs.jmedchem.1c02179>.
- [40] K. Yang, H. Wu, Z. Zhang, E.D. Leisten, X. Nie, B. Liu, Z. Wen, J. Zhang, M. D. Cunningham, W. Tang, Development of Selective Histone Deacetylase 6 (HDAC6) Degraders Recruiting Von Hippel-Lindau (VHL) E3 Ubiquitin Ligase, *ACS Med Chem Lett* 11 (4) (2020) 575–581, <https://doi.org/10.1021/acsmchemlett.0c00046>.
- [41] J.P. Smalley, G.E. Adams, C.J. Millard, Y. Song, J.K.S. Norris, J.W.R. Schwabe, S. M. Cowley, J.T. Hodgkinson, PROTAC-mediated degradation of class I histone deacetylase enzymes in corepressor complexes, *Chem Commun (Camb)* 56 (32) (2020) 4476–4479, <https://doi.org/10.1039/d0cc01485k>.
- [42] K. Yang, Y. Zhao, X. Nie, H. Wu, B. Wang, C.M. Almodovar-Rivera, H. Xie, W. Tang, A Cell-Based Target Engagement Assay for the Identification of Cereblon E3 Ubiquitin Ligase Ligands and Their Application in HDAC6 Degraders, *Cell Chem Biol* 27 (7) (2020) 866–876 e8, <https://doi.org/10.1016/j.chembiol.2020.04.008>.
- [43] L. Sinatra, J. Yang, J. Schliehe-Diecks, N. Dienstbier, M. Vogt, P. Gebing, L. M. Bachmann, M. Sonnichsen, T. Lenz, K. Stuhler, A. Scholer, A. Borkhardt, S. Bhatia, F.K. Hansen, Solid-Phase Synthesis of Cereblon-Recruiting Selective Histone Deacetylase 6 Degraders (HDAC6 PROTACs) with Antileukemic Activity, *J Med Chem* (2022), <https://doi.org/10.1021/acs.jmedchem.2c01659>.

- [44] J. Chotitumnavee, Y. Yamashita, Y. Takahashi, Y. Takada, T. Iida, M. Oba, Y. Itoh, T. Suzuki, Selective degradation of histone deacetylase 8 mediated by a proteolysis targeting chimera (PROTAC), *Chem Commun (Camb)* 58 (29) (2022) 4635–4638, <https://doi.org/10.1039/d2cc00272h>.
- [45] S. Darwish, E. Ghazy, T. Heimburg, D. Herp, P. Zeyen, R. Salem-Altintas, J. Ridinger, D. Robaa, K. Schmidtkunz, F. Erdmann, M. Schmidt, C. Romier, M. Jung, I. Oehme, W. Sippl, Design, Synthesis and Biological Characterization of Histone Deacetylase 8 (HDAC8) Proteolysis Targeting Chimeras (PROTACs) with Anti-Neuroblastoma Activity, *Int J Mol Sci* 23 (14) (2022), <https://doi.org/10.3390/ijms23147535>.
- [46] Z. Sun, B. Deng, Z. Yang, R. Mai, J. Huang, Z. Ma, T. Chen, J. Chen, Discovery of pomalidomide-based PROTACs for selective degradation of histone deacetylase 8, *Eur J Med Chem* 239 (2022), 114544, <https://doi.org/10.1016/j.ejmech.2022.114544>.
- [47] J. Huang, J. Zhang, W. Xu, Q. Wu, R. Zeng, Z. Liu, W. Tao, Q. Chen, Y. Wang, W. G. Zhu, Structure-Based Discovery of Selective Histone Deacetylase 8 Degradators with Potent Anticancer Activity, *J Med Chem* (2022), <https://doi.org/10.1021/acs.jmedchem.2c00739>.
- [48] X. Han, Y. Sun, Strategies for the discovery of oral PROTAC degradators aimed at cancer therapy, *Cell Reports Physical Science* 3 (10) (2022), <https://doi.org/10.1016/j.xcrp.2022.101062>.
- [49] I. Sosic, A. Bricelj, C. Steinebach, E3 ligase ligand chemistries: from building blocks to protein degradators, *Chem Soc Rev* 51 (9) (2022) 3487–3534, <https://doi.org/10.1039/d2cs00148a>.
- [50] M.D. Hartmann, I. Boichenko, M. Coles, F. Zanini, A.N. Lupas, B. Hernandez Alvarez, Thalidomide mimics uridine binding to an aromatic cage in cereblon, *J Struct Biol* 188 (3) (2014) 225–232, <https://doi.org/10.1016/j.jsb.2014.10.010>.
- [51] J. Cheng, Y. Li, X. Wang, G. Dong, C. Sheng, Discovery of Novel PDEdelta Degradators for the Treatment of KRAS Mutant Colorectal Cancer, *J Med Chem* 63 (14) (2020) 7892–7905, <https://doi.org/10.1021/acs.jmedchem.0c00929>.
- [52] K. Moreau, M. Coen, A.X. Zhang, F. Pachi, M.P. Castaldi, G. Dahl, H. Boyd, C. Scott, P. Newham, Proteolysis-targeting chimeras in drug development: A safety perspective, *Br J Pharmacol* 177 (8) (2020) 1709–1718, <https://doi.org/10.1111/bph.15014>.
- [53] M. Petterson, C.M. Crews, PROTeolysis TArgeting Chimeras (PROTACs) - Past, present and future, *Drug Discov Today Technol* 31 (2019) 15–27, <https://doi.org/10.1016/j.ddtec.2019.01.002>.
- [54] M. Kostic, L.H. Jones, Critical Assessment of Targeted Protein Degradation as a Research Tool and Pharmacological Modality, *Trends Pharmacol Sci* 41 (5) (2020) 305–317, <https://doi.org/10.1016/j.tips.2020.02.006>.
- [55] G.M. Morris, R. Huey, W. Lindstrom, M.F. Sanner, R.K. Belew, D.S. Goodsell, A. J. Olson, AutoDock4 and AutoDockTools4: Automated docking with selective receptor flexibility, *J Comput Chem* 30 (16) (2009) 2785–2791, <https://doi.org/10.1002/jcc.21256>.
- [56] S. Forli, R. Huey, M.E. Pique, M.F. Sanner, D.S. Goodsell, A.J. Olson, Computational protein-ligand docking and virtual drug screening with the AutoDock suite, *Nat Protoc* 11 (5) (2016) 905–919, <https://doi.org/10.1038/nprot.2016.051>.